An updated genetic model for metamorphosed and deformed, c. 1.89 Ga magnesian Zn-Pb-Ag skarn deposits, Sala area, Bergslagen, Sweden

Nils F Jansson
Luleå University of Technology

Rodney L Allen
Volcanic Resources AB

Göran Skogsmo, Nils Vorbrodt, Mattias Bäckström
Björka mineral AB

Abstract. This contribution presents an updated view on the genesis of stratabound Zn-Pb-Ag mineralization in the Sala area, Bergslagen, Sweden. Integrated legacy and new geological, geochemical and geophysical data reveal that the deposits are hosted by a complex array of magnesian skarn-altered zones in dolomitic marble. These mineralized zones parallel early faults and metavolcanic interbeds in the host marble, and converge downwards in the stratigraphy adjacent to a 1.89 Ga calc-alkaline granite-granodiorite batholith. Prograde alteration involved formation of early barren ferroan diopside- and forsterite-bearing skarns. Mineralization is mainly associated with subsequent alteration to tremolite, chlorite, serpentine, magnetite and calcite. The hydrous associations overlap mineralogically with assemblages formed during subsequent greenschist facies regional metamorphism between 1.87 Ga and 1.8 Ga. However, ferroan diopside and forsterite are unique to the alteration system, and indicate mineralization in conjunction with an early, high T, metasomatic alteration event at 1.89 Ga. The Sala deposits can be classified as Zn skarn deposits, albeit atypical in the magnesian nature of the skarns and the lack of minerals with essential Mn. The Fe and Mn content in magnesian silicates and carbonates is however sufficient to induce clear enrichment haloes of these elements around the deposits. The magnesian nature of the skarns probably reflect formation in a shallow marine continental back-arc tectonic setting, and an importance of seawater in early pre-skarn alteration stages, such as dolomitization.

1 Introduction

The Sala area is one of the classic mining areas in the Bergslagen mining district of southern Sweden. Several stratabound polymetallic sulphide deposits are hosted by dolomitized and hydrothermally altered stromatolitic limestone, including the c. 5 Mt Sala Zn-Pb-Ag deposit; Sweden's most historically important silver mine. The marble unit has also been mined for calcite and dolomite, and high quality dolomite for industrial applications is still mined at Tistbrottet directly west of Sala mine (Fig. 1).

The Sala deposit belongs to a sub-type of stratabound marble- and skarn-hosted deposits in Bergslagen. Current understanding based on field evidence and cross-cutting relationships suggest these deposits formed in an early, subseafloor setting at c. 1.89 Ga, when submarine strata were buried and intruded by porphyritic rocks and granitoids. The deposits have many mineralogical and textural similarities to metasomatic skarn deposits (e.g. Allen et al. 2003; Jansson and Allen 2015). However, an overprint by regional metamorphism and deformation during the Svecokarelian orogeny at 1.87-1.80 Ga complicate ore genetic interpretation, in particular the distinction between early ore-related silicates and silicates formed during the regional metamorphic overprint. Analogous to classic discussions on the genesis of Broken Hill-type deposits, metamorphism has induced uncertainty on whether minerals such as diopside and garnet formed metasomatically in conjunction with ore formation, or later when lower temperature alteration assemblages were metamorphosed.

The Sala area is particularly favorable for addressing this problem, since the metamorphic grade only reached upper greenschist facies, as opposed to amphibolite or granulite facies elsewhere in Bergslagen. Furthermore, the area contains some of the most texturally well-preserved rocks in the region. This contribution presents an updated genetic model based on a recent drill core logging and mapping campaign complemented by microscopy and analysis of numerous samples for whole-rock lithogeochemistry and mineral chemistry.

2 The Sala Area

The Sala area is located in the central part of Bergslagen. It is dominated by c. NW-trending, gently plunging F_1 folds that are overprinted by open, NE-trending F_2 folds. The eastern part of Fig. 1 is characterized by zigmoidal, parasitic F_1 folds whereas the western part is a culmination of F_1 folds, interpreted as a F_1 synclinorium. The western limb of this synclinorium is truncated by a prominent, WSW-dipping shear zone with inferred dextral and reverse displacement.

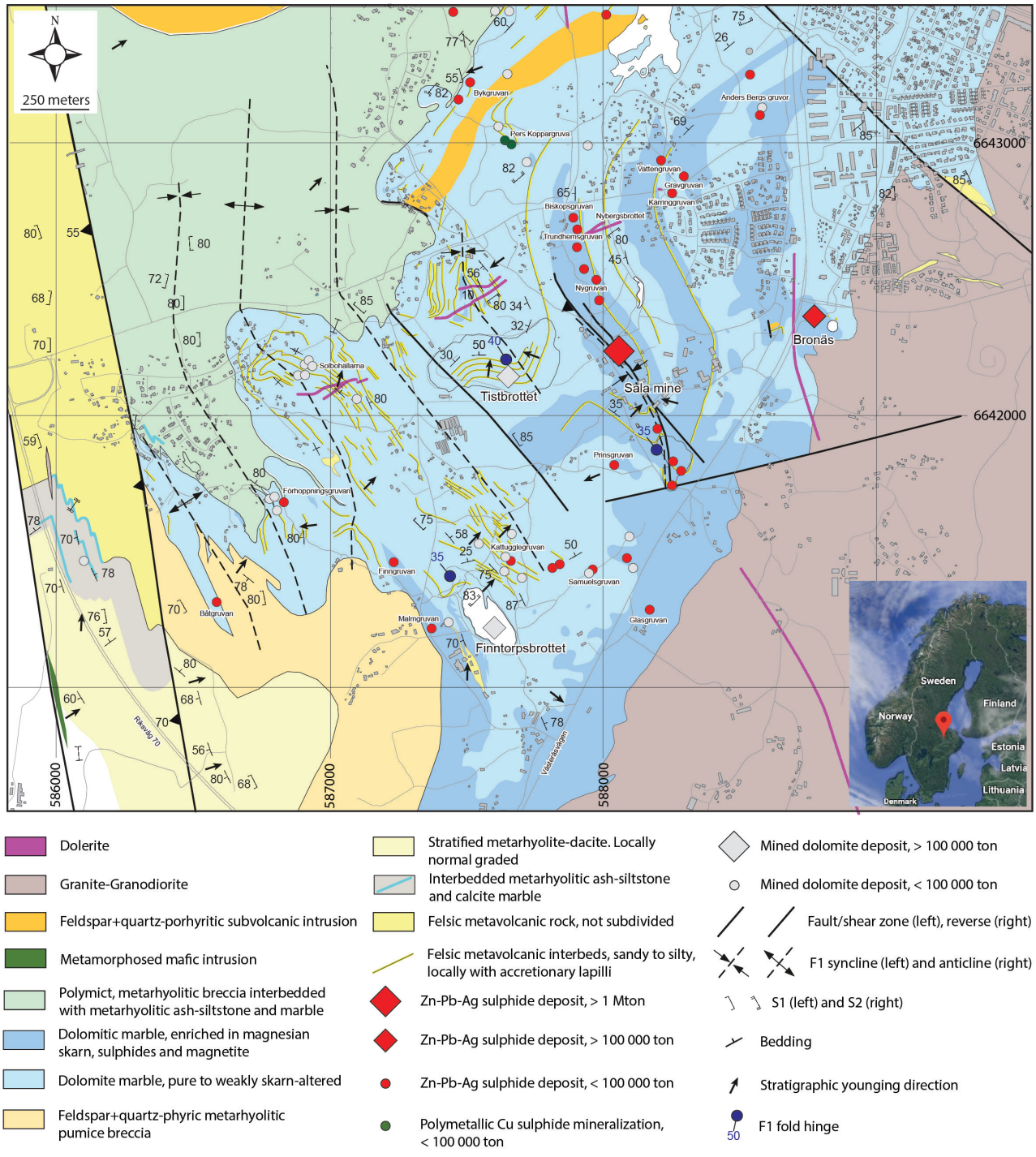

Figure 1. Revised bedrock geological map of the Sala area based on new mapping and compilation of legacy data (incl. an unpublished map by Eriksson and Åhman (1961). Trace of skarn-altered zones is based on mapping, drill core logging and legacy ground magnetic data. Note convergence of the skarn-altered zones against the western contact of the Sala-Vänge granitoid. Grid is SWEREF 99TM. Lower right inset shows location of Sala in Sweden.

Towards the east, the marble unit is truncated by a large calc-alkaline granite-granodiorite batholith; the Sala-Vänge batholith. Ripa et al. (2002) presented two ages of 1891±6 and 1890±6 Ma of magmatic crystallization, overlapping within error with the age of a dated volcaniclastic interbed in the marble. Shearing and granitoid emplacement have led to that metavolcanic rocks belonging to the original stratigraphic footwall being only present in the SW part of Figure 1. In terms of original volcanic facies, the footwall can be subdivided into a lower succession of stratified, rhyolitic-dacitic siltstone-sandstone with local volcaniclastic breccia intervals and an upper c. 300 m thick unit of feldspar+quartz-phyric rhyolitic pumice breccia. Deposition of the limestone (now marble) occurred during a lowstand in volcanism during which

growth of stromatolitic limestone was intermittently interrupted by deposition of resedimented volcaniclastic debris (Allen et al., 2003). A succession of metamorphosed polymict rhyolitic volcanic breccia-conglomerate and rhyolitic silt-sandstone overlie the marble. The breccia-conglomerate units commonly have erosional lower contacts and locally carry clasts of former limestone. Pumice clasts become more common stratigraphically up-section.

3 The alteration system

The sulphide deposits mainly occur as breccia infill, vein networks and disseminations in skarn-rich dolomitic marble (Fig 2A). Jansson (2017) showed that sulphides have locally replaced and mimicked original stromatolitic laminae. The main ore minerals are sphalerite and galena accompanied by pyrrhotite and pyrite. A plethora of Ag-, Sb- and Hg-bearing minerals accompany the base metal sulphides, such as freibergite, silver amalgam, dyscrasite, miargyrite, allargentum, pyrargyrite gudmundite, boulangerite and geocronite (Kieft et al. 1987).

The gangue minerals are tremolite, calcite, phlogopite, chlorite, serpentine, talc, ferroan diopside, locally barite, magnetite and very rarely grossular-andradite garnet and dravite tourmaline. Dolomitic marble carrying associations of these minerals define c. 200 m wide haloes around most known deposits (Fig. 1). These haloes coincide with weak but consistent whole-rock Fe and Mn enrichments and positive magnetic anomalies imparted by ubiquitous accessory magnetite and pyrrhotite. Using these geochemical and geomagnetic criteria, complex branching geometries are suggested for the alteration system, ranging from discordant to semi-concordant relative to stratigraphy. Jansson (2017) showed that this pattern reflects a combination of cross-stratal fluid flow along early faults and fluid flow along the contacts of numerous volcanic interbeds in the limestone precursor. F_1 folding transposed these alteration zones with the result that they are now sub-parallel in plan view. The alteration zones converge down-stratigraphy and towards the contact of the Sala-Vänge granitoid (Fig.1).

Clinopyroxene-bearing skarns occupy a central position in the altered zones, including Glasgruvan (Fig.1) which is the type-locality of the eponymous ‘salite’; an old term for ferroan diopside. Locally, clinopyroxene can be seen to have formed as an open-space infilling in zoned vein networks and breccias where it exhibits a bladed habit (Fig 2B). Early clinopyroxene display complex growth zoning, reflecting variable Fe, Mg and Mn contents ($Di_{66.6}Hd_{25.7}Jhn_{7.7}$-$Di_{96.6}Hd_{2.8}Jhn_{0.6}$, Fig. 2C).

More peripheral in the haloes, forsterite ($Fo_{94}Fay_5$-$Fo_{96}Fay_4$) is the main anhydrous skarn mineral; a mineral which hitherto has been neglected at Sala (Fig. 2D). The reason for this is most likely the common alteration of salite and forsterite to hydrous associations of tremolite, serpentine, chlorite, talc, magnetite and calcite (e.g. Fig. 2A), which are now dominant.

Sphalerite is locally observed in textural equilibrium with a younger generation of ferroan diopside in veins cross-cutting earlier salite skarns, and cm-sized clinopyroxene and more rarely garnet ($Grs_{61}Adr_{21}Sps_8$) were found in the massive sulphide ore (cf. Sjögren, 1910). However, most sulphide mineralization is associated with hydrous minerals; e.g. sphalerite and tremolite replacing earlier clinopyroxene (Fig. 2A) or dolomite directly (Fig. 2B). Galena and pyrrhotite commonly occur in association with tremolite, serpentine, chlorite and minor magnetite replacing forsterite porphyroblasts (Fig. 2D). The altered dolomite and the magnesian silicates have elevated Fe and Mn, and the associated magnetite carry up to 3.10 wt.% MnO. This is the mineralogical manifestation of aforementioned geochemical and magnetic haloes. However, minerals with essential Mn are lacking at Sala.

Sjögren (1910) found that the ore sulphides have locally perfectly pseudomorphed fibrous tremolite crystals, further highlighting the link between mineralization and retrograde alteration. However, the final stages of retrograde alteration appear to have been barren, except for with respect to amalgams, antimonides and native forms of Ag, Sb and Hg (e.g. Kieft et al. 1987). In Sala mine, this is best reflected by transgressive zones of talc, serpentine and chlorite that occupy a central part of the mineralized system, yet are essentially barren. The strong spatial relationship of these zones to ore have led most observers to interpret them as fossil conduits for hydrothermal fluids (e.g. Sjögren 1910, Jansson 2017). Their barren nature most likely reflect focused retrograde alteration by highly reactive, acidic and siliceous fluids that were poor in metals and/or sulphur. The high content of mechanically weak silicates in these zones resulted in ductile shear zones during subsequent deformation. Strain partitioning by these zones may be the reason why relatively well-preserved rocks can be found in the area near the Sala mine and adjacent dolomite mines.

The Sala-Vänge batholith has a sharp contact towards the alteration system, but is itself virtually unaltered. At the Bronäs deposit (Fig. 1), irregular bodies of weakly sericite-altered feldspar+quartz-porphyritic rocks with chilled margins intruded highly altered and mineralized dolomitic marble directly adjacent to sulphide mineralization. These features can be reconciled if emplacement of these intrusions post-dated mineralization, yet occurred along the same structures that originally channeled the mineralizing fluids.

4 Conclusions

Despite the tectonometamorphic overprint, we recognize that intrusive-related, metasomatic processes were involved in the genesis of the polymetallic sulphide mineralization in the Sala area. The common association of sulphides with retrograde minerals is similar to typical metasomatic skarn deposits (e.g. Meinert et al. 2005). Similar to Zn skarns worldwide, the Sala deposits appears to be structurally controlled and

to have formed away from intrusive contacts. On the other hand, the skarn parageneses are more magnesian than in typical Zn skarn deposits, which typically formed in calcitic rocks and where the alteration silicates are more Fe- and Mn-rich. Most likely, these differences reflect the unusual submerged, intra-continental back-arc tectonic setting of skarn deposits in Bergslagen. This meant involvement of modified seawater in early, pre-skarn alteration stages, such as dolomitization of original calcitic limestone and hydrothermal alteration of volcanic rocks. Nevertheless, the Sala deposits can be included in the larger family of Zn skarn deposits as defined by e.g. Meinert et al. (2005). The results support other studies elsewhere in Bergslagen (e.g. Jansson and Allen, 2015), concluding that despite the complex regional metamorphic overprint, contact metasomatic processes related to 1.89 Ga intrusions can still be recognized.

Acknowledgements

This research was carried out as part of the Strategic Innovation Programme for the Swedish Mining and Metal Producing Industry (STRIM) of VINNOVA, Formas and the Swedish Energy Agency, with additional financial support from Boliden and Björka Mineral. Beowulf Mining is thanked for providing access to an exploration drill core from the Sala area.

References

Allen RL, Bull S, Ripa M, Jonsson R (2003) Regional stratigraphy, basin evolution, and the setting of stratabound Zn–Pb–Cu–Ag–Au deposits in Bergslagen, Sweden. Final report for SGU-FoU project 03-1203/99, jointly funded by SGU and Boliden Mineral AB

Eriksson, T., Åhman, E (1961) Geologisk karta över området vid Sala gruva. Unpublished 1:5000 map, Björka Mineral archive, Sala.

Jansson NF, Allen RL (2015) Multistage ore formation at the Ryllshyttan marble and skarn-hosted Zn-Pb-Ag-(Cu) + magnetite deposit, Bergslagen, Sweden. Ore Geol Rev 69:217-242

Jansson NF (2017) Structural evolution of the Palaeoproterozoic Sala stratabound Zn-Pb-Ag deposit, Bergslagen, Sweden. GFF 139:21-35

Kieft C, Holmgren J, Eriksson, G (1987) The silver-mercury-antimony minerals of Sala, Sweden. Canadian Mineralogist 25:647-658

Meinert LD, Dipple, GM, Nicolescu S (2005) World skarn deposits. In: Hedenquist JW, Thompson JFH, Goldfarb RJ, Richards JP (eds) Economic geology 100th Anniversary volume 1905–2005:299-336

Ripa M, Kubler L, Persson L, Göransson M (2002) Beskrivning till berggrundskartan och bergkvalitetskartan 11G Västerås NO. Geol Survey Sweden Af 217, 70 pp.

Sjögren HJ (1910) The Sala mine. Geologiska Föreningen i Stockholm Förhandlingar 32:1363-13

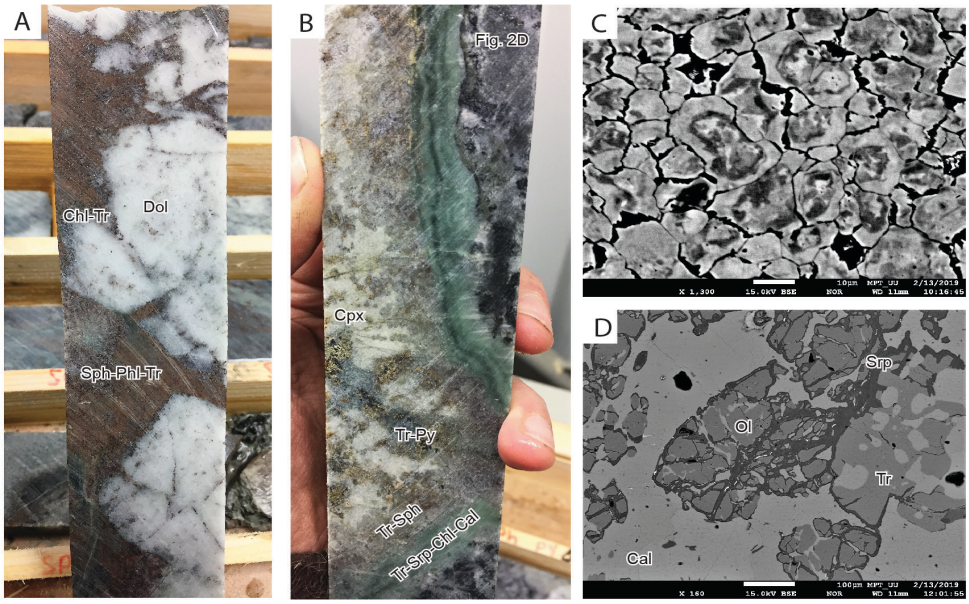

Figure 2. Examples of skarn and mineralization parageneses in the Sala area. A) Breccia-type ore with dolomite marble clasts cemented by sphalerite, tremolite and phlogopite. B) Clinopyroxerne skarn pod in olivine-porphyroblastic dolomitic marble. Clinopyroxene is irregularly replaced by tremolite and sulphides whereas olivine have calcite haloes and are replaced by serpentine, sulphide and magnetite. The laminated zones consist of fine-grained intergrowths of the hydrous minerals and calcite. C) Barren, pre-sulphide clinopyroxene skarn from Glasgruvan; type-locality of salite. A core of ferroan diopside (light) is overgrown and partly replaced by diopside (dark grey), in turn followed by a rim of younger ferroan diopside. D) Forsterite variably replaced by serpentine and accessory magnetite and pyrrhotite.

Stanniferous silicates in an exotic scheelite skarn close to the Felbertal tungsten mine, Eastern Alps, Austria

Johann G. Raith, Alexander Ordosch
Montanuniversität Leoben, Austria

Abstract. A unique type of W-(Sn) skarn mineralisation is reported from a tungsten prospect about 8 km south of Felbertal scheelite mine in the Alps. Scheelite is hosted in calc-silicate rocks consisting of stanniferous clinozoisite, quartz, plagioclase, calcite and chlorite. Tin is exclusively incorporated in the lattice of clinozoisite and titanite. Concentrations of up to 3.00 mass% SnO_2 in clinozoisite are the highest values recorded for this mineral so far. Substitution of $(Al, Fe)^{3+}$ by $(Sn, Ti)^{4+}$ in clinozoisite is balanced by incorporation of Fe^{2+}. The skarn assemblage records a regional metamorphic overprint. Formation as a distal magmatic skarn is discussed.

1 Introduction

Tungsten exploration in the 1960s to 1980s in the Eastern Alps resulted in discovery of numerous scheelite showings but also of the world-class Felbertal scheelite deposit (annual production 2016 1200 t WO_3). A peculiar aspect of scheelite mineralisation in the Eastern Alps is the paucity of Sn. Mineralised systems containing Sn in addition to W are extremely rare; e.g., only traces of Sn are found in the Felbertal deposit and Sn is lacking in all other scheelite occurrences in the Eastern Alps.

A remarkable exception to this is Messelingscharte (~8 km S of Felbertal) that was re-explored in 2015 by Wolfram Bergbau und Hütten AG. There, the main mineralisation is a Sn-bearing scheelite skarn, which was not identified correctly when it was discovered in the 1960s. The particular feature is that Sn is hosted in Ca-silicate minerals and not in cassiterite.

This study presents information on the geological setting, the skarn petrography and mineralogical data of the stanniferous silicates. Sn-bearing silicates are known from magmatic skarn deposits, but there are very few comparable examples documented in the international literature. It will be argued that this mineralisation type is comparable to distal granite-related magmatic skarns.

2 Geological setting

The study area is situated in the central Tauern Window in the Eastern Alps. The geological units relevant for W-(Sn) mineralisation are metamorphosed Cambro-Ordovician basement units and Permo-Carboniferous metagranites (Zentralgneis). The pre-Variscan metamorphic units include two metabasite dominated units, the Basal Amphibolite (Basisamphibolit) and the Habach Complex that are separated by the Basal Schist unit.

The Basal Amphibolite comprises amphibolites and meta-gabbros of debated protolith age (pre-Variscan vs. Variscan) showing enriched MORB-like geochemical signatures typical of back-arc magmas (Ordosch 2017; Vavra and Frisch 1989). The overlying metavolcano-sedimentary sequence is referred to as the Basal Schist (Basisschiefer). The poly-metamorphic Habach Complex consists of various pre-Variscan meta-igneous rocks, clastic metasediments and Variscan meta-granitoids (e.g. Höck 1993). It is subdivided into the Lower Magmatic Series (LMS), Upper Magmatic Series (UMS) and the Habach phyllite. The Lower Magmatic Series, a dismembered meta-ophiolite, consists of amphibolites, metagabbros, meta-ultramafic rocks and minor meta-sediments and Early Cambrian I-type metagranitoids (Höll and Eichhorn 2000). The Upper Magmatic Series is an arc sequence including various metamorphosed basic to acidic calc-alkaline volcanic rocks grading into the Habach phyllites.

The Felbertal tungsten deposit consists of a metamorphosed stockwork of deformed quartz-scheelite veins, mineralised shear zones with strongly foliated quartz-scheelite ores and disseminated scheelite mineralisation in the host rocks. It was interpreted as a polygenetic strata-bound scheelite deposit (Höll and Eichhorn 2000). A conspicuous orthogneiss ("K1 Gneis") derived from an evolved 340 Ma granite played a key role in formation of the Felbertal deposit (see review in Raith et al. 2018).

3 W-(Sn) skarn mineralisation

Scheelite is predominantly present in massive, non-foliated clinozoisite-rich calcic skarn rock and amphibole schist. The skarn bodies occur as irregular pods and nests up to 2.0 x 1.5 m in size within the amphibolites of the Basal Amphibolite unit. The skarn is composed of clinozoisite (50%), quartz (20%), plagioclase (15%), scheelite (6%), calcite (5%) and minor to accessory chlorite, titanite, apatite, zircon, pyrite and chalcopyrite. Two types of clinozoisite can be distinguished. Clinozoisite 1 is coarse-grained forming prismatic to irregular subhedral crystals. The assemblage is stanniferous clinozoisite + scheelite + (stanniferous) titanite + quartz + plagioclase + calcite. Clinozoisite 2 is finer-grained and occurs in the assemblage clinozoisite + chlorite + quartz ± calcite; it often forms euhedral crystals inter-grown with quartz. The minerals show a mosaic texture indicative of metamorphic re-crystallisation. Transitions of Clinozoisite 1 to 2 are also documented.

Titanite is fine- to medium-grained forming euhedral (sphenoidal) to anhedral, granular textured grains. Euhedral titanite is very common at the contact of the skarn rock to amphibole. Scheelite is of variable grain size and shows blue to yellow fluorescence under short wave UV light. Larger scheelite crystals may show undulose extinction and optical zoning. Normally, the core of larger scheelite crystals is yellow fluorescent grading into a blue rim.

Amphibole schist forming thin (cm) irregular, discontinuous layers is commonly associated with the skarn, especially at the contact with the host amphibolite. It is composed of medium-grained hornblende (50%), quartz (30%) and biotite (20%). Accessory minerals are pyrite, apatite, scheelite, chlorite and titanite. In addition to the skarn, scheelite has also been observed in deformed scheelite quartz veins/veinlets and stringers hosted in foliated amphibolite and in mylonitic quartz veins.

4 Sn-bearing silicates

4.1 Clinozoisite

Mineral chemical compositions were analysed by EPMA in WDS mode at Montanuniversität Leoben; for analytical conditions see Ordosch (2017). Clinozoisite is characterised by an average molar Al/Fe^{3+} of 4.4 and Sn contents reach up to 3.0 mass% SnO_2. Concentrations of Na_2O, K_2O and MgO are generally very low, MnO can reach up to 0.67 mass% and TiO_2 up to 1.60 mass%.

Petrography and mineral chemical data allow distinction of two types of clinozoisite. Clinozoisite 1 comprising coarse-grained, irregular grains is higher in Sn and often shows an irregular intra-grain zoning (Fig. 1). High Sn/Ti domains normally occur as relict intra-grain domains that are incompletely replaced or overgrown by low-Sn clinozoisite (Clinozoisite 2); the latter also forms distinct euhedral, small crystals that clearly represent newly formed metamorphic grains. These grains are Sn-poor/free and there is no internal chemical zonation visible. Clinozoisite displays two chemical populations. The low-Sn population is characterised by ≤0.3 mass% SnO_2 (=0.01 apfu Sn; typical values 0-0.1 mass%). The high-Sn population reaches values of 3.00 mass% SnO_2 (=0.094 apfu; typical values 0.5-1 mass%). The high-Sn population mostly corresponds to Clinozoisite 1.

From crystal chemical considerations it is assumed that Sn^{4+} and Ti^{4+} are incorporated at the octahedral sites of clinozoisite/epidote where they may substitute for (Al, $Fe)^{3+}$ at the M3 site. For charge balance equivalent amounts to Sn^{4+} and Ti^{4+} of divalent cations must be incorporated according to the following substitution: $2(Al,Fe)^{3+} \Leftrightarrow (Sn,Ti)^{4+} + (Fe,Mg,Mn)^{2+}$.

4.2 Titanite

Titanite mineral formulae were calculated on the basis of 1 Si + OH. In backscatter electron images titanite shows patchy irregular internal zoning (Fig. 3). Occasionally, micro-inclusions of cassiterite are observed. The patchy zoning is defined by element variations between Sn-Al-rich and Ti-Fe-rich intra-grain domains. Comparable irregular patchy zoning has been reported from zircons. It can be explained as disequilibrium texture caused by in-situ fluid-related mineral dissolution-precipitation during metamorphism. By this process earlier formed Sn-rich titanite transforms to Sn-poor titanite.

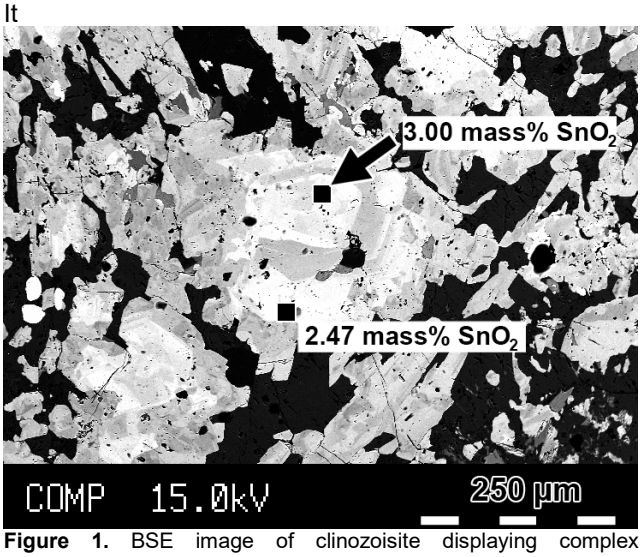

Figure 1. BSE image of clinozoisite displaying complex intergrowths and zoning. The bright domains/zones are high in SnO_2.

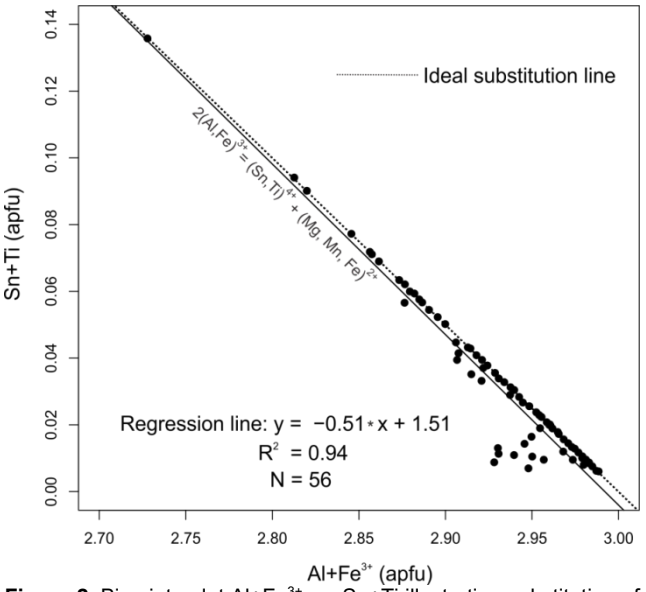

Figure 2. Bivariate plot Al+Fe^{3+} vs. Sn+Ti illustrating substitution of Sn in clinozoisite; Atoms per formula unit (apfu) calculated based on 12.5 oxygens. Dashed line represents the ideal substitution line. Calculated regression line is identical with the ideal substitution line for 95% confidence.

Values of x_{Al} = Al/(Al+Fe+Ti+Sn) for titanite range from 0.075-0.236 with a median of 0.125; i.e. all titanites are classified as low-Al titanites. Titanite has a very variable content of SnO_2 ranging from 0.07 to 6.48 mass% (median 2.29 mass%). Statistically only one population of titanite can be identified in the data set.

Incorporation of Sn is according to simple $Sn^{4+} \Leftrightarrow Ti^{4+}$ substitution; i.e. solid solution of titanite-malayaite $CaSnSiO_4(O,OH,F)$ (Takenouchi 1971).

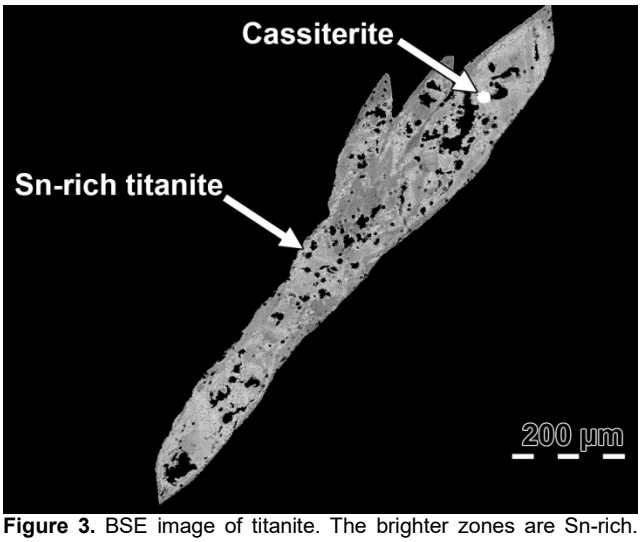

Figure 3. BSE image of titanite. The brighter zones are Sn-rich. Arrow points out micro-inclusion of cassiterite (white).

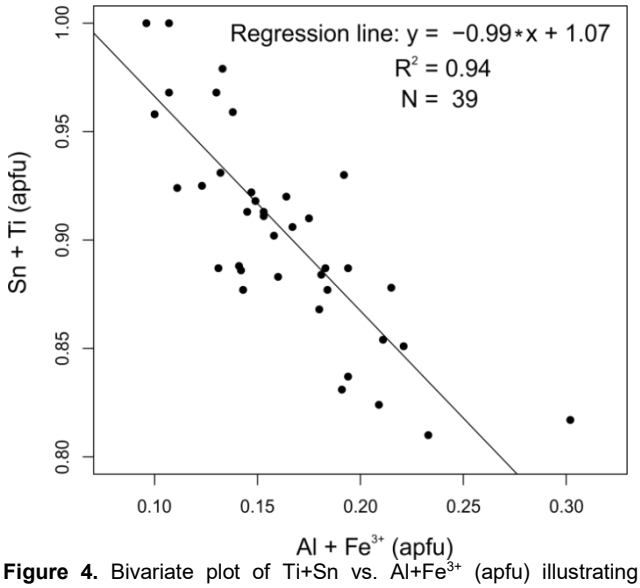

Figure 4. Bivariate plot of Ti+Sn vs. $Al+Fe^{3+}$ (apfu) illustrating substitution of Sn in titanite.

The F concentrations of titanite range between 0.5-1.6 mass% (median 1.1 mass%; 0.12 apfu). Substitution of F in titanite is via (Ribbe 1982):
$(Al,Fe)^{3+} + (OH,F)^{-} \Leftrightarrow Ti^{4+} + O^{2-}$. The titanites analysed show a good negative correlation of F with Ti. Al and Fe are the main cations substituting for Ti (+Sn) (Fig. 4). The substitution of Sn for Ti is coupled with preferred incorporation of Fe^{3+} for Al^{3+} (WDS element mappings, not shown).

5 Discussion

5.1 Comparison with other localities

As documented in this study, clinozoisite from Messelingscharte incorporates high quantities of Sn^{4+}. The maximum analysed is 3.00 mass% SnO_2 (=0.094 apfu), which is the highest value ever recorded in the literature to the knowledge of the authors. Worldwide, only a few other occurrences of Sn-bearing clinozoisite/epidote are known. Stanniferous clinozoisite/epidote was reported from massive skarns and skarn veins in Cornwall, UK (Alderton and Jackson 1978; van Marcke de Lummen 1986) and Cassiar district, British Columbia, Canada (Mulligan and Jambor 1968).

Tin-bearing calc-silicate bodies and veins were described from the St. Just aureole in the Land's End granite, Cornwall (Alderton and Jackson 1978). The irregular-shaped discordant calc-silicate bodies and veins are composed of Ca-rich garnet, diopside, hornblende, epidote, ± axinite, ± tourmaline, ± accessory calcite, quartz, titanite and sulphides.

Tin-bearing epidote from the Chycornish Carn skarn vein is associated with hornblende, axinite, tourmaline and accessory titanite etc. Cassiterite is generally absent in all these calc-silicate veins and the Sn carriers are silicates. The skarn veins were interpreted as high-temperature (c. 500°C) metasomatic rocks predating Cu-Sn mineralisation in the tin lodes. An external; i.e. granitic, source of elements like Sn and Be has been envisaged.

Sn-bearing clinozoisite (up to 2.84 mass% SnO_2) was moreover described from The Crowns, also in the contact aureole of the Land's End granite. There, it is part of the retrograde skarn assemblage including stanniferous epidote, cassiterite, amphibole, titanite/malayaite and chlorite and overprinting earlier grossular/andradite-rich skarn (van Marcke de Lummen 1986).

Stanniferous epidote has been reported from Fe-rich pyroxene skarns in the Cassiar district, British Columbia, Canada. These tin skarns belong to a mineralised belt with several Be, Sn, W and Mo occurrences that are spatially linked with granite batholiths in the Western Cordillera. The main constituents are Sn-bearing clinopyroxene, amphibole, epidote, garnet, calcite, quartz and accessory titanite; tin is incorporated in andradite, malayaite, epidote and amphibole (Mulligan and Jambor 1968; Scribner et al. 2017). Interestingly, at none of these localities scheelite has been reported as part of the Sn-bearing assemblage and even cassiterite is rare.

All these reported skarns are connected to granite-related magmatic hydrothermal systems. It is therefore tempting to postulate a similar genesis for Messelingscharte although there are no geological indications for a nearby intrusive contact there. However, it must be kept in mind that the Cornish Sn-(W) granites are post-orogenic whereas in the central Tauern Window pre-Alpine W-(Sn) mineralisation has been overprinted by Alpine tectonics and regional metamorphism. Thus, the Alpine orogeny likely blurred many of the primary features.

5.2 Processes of skarn formation

Calc-silicate rocks, often collectively referred to as skarns, can form in different geologic environments by

various processes: isochemical formation of calc-silicate rocks with internal fluid buffering, local fluid exchange at the contacts between shales and limestones producing reaction skarns reactions and finally true magmatic skarns with infiltration of external magmatic hydrothermal fluids (e.g. Einaudi et al. 1981).

This ambiguity is especially true for scheelite bearing calc-silicate rocks. In addition to magmatic tungsten skarns there are smaller sub-economic tungsten deposits in regional metamorphic calc-silicate rocks unrelated to granites (e.g., Eastern Alps, Raith 1991).

However, the vast majority of W mineralised calc-silicate rocks are magmatic tungsten skarns commonly forming proximal calcic exoskarns but also distal skarns developed along faults and major shear zones. Such magmatic W skarns (e.g., Cantung, Canada or King Island, Australia) are typically associated with evolved granites but they are normally Sn-free (Meinert et al. 2005). In Sn-W-F-Be skarns Sn may be incorporated in silicates (titanite, garnet, amphibole, ilvaite) during the later skarn stages (e.g. Mt. Lindsey, Australia, Kwak 1983).

The mineral assemblage of the clinozoisite-dominated skarn at Messelingscharte is comparable to lower temperature (retrograde) skarn assemblages. The lack of the high-temperature garnet-clinopyroxene assemblages can be explained with the distal position of skarn formation which is further corroborated by the lack of a contact aureole and nearby granite intrusion. The regional geological setting of Messelingscharte also supports the model of distal skarn formation. Discordant scheelite-bearing quartz veins and stringers could represent feeder zones for skarn-forming magmatic hydrothermal fluids.

The world-class Felbertal scheelite deposit is located only about 8 km north of Messelingscharte. Recent studies confirmed the Variscan age of this deposit and the genetic link with c. 335-340 Ma evolved granites (K1 Gneis) in the deposit (Kozlik et al. 2016). The hypothesis that the W deposit Felbertal and W-(Sn) mineralisation at Messelingscharte are part of a common magmatic-hydrothermal system related to Variscan magmatism has still to be tested in the future.

6 Implications

The unique W-(Sn) skarn reported here is the first record of scheelite mineralisation associated with tin in the Eastern Alps. Tin is exclusively incorporated in the lattice of clinozoisite and titanite and not present as cassiterite; thus, it is difficult to detect during exploration. The element association W-Sn supports a granitic provenance of the ore forming fluids thereby supporting magmatic-hydrothermal models of W mineralisation in the Felbertal area.

Acknowledgements

Wolfram Bergbau und Hütten AG, namely S. Schmidt and K. Aupers, are thanked for providing logistic and financial support. M. Zimmermann and F. Zaccarini, Montanuniversität Leoben, are thanked for sample preparation and help with the EPMA analyses.

References

Alderton DHM, Jackson NJ (1978) Discordant calc-silicate bodies from the St. Just aureole, Cornwall. Mineral Mag 42:427-434.

Einaudi MT, Meinert LD, Newberry RJ (1981) A special issue devoted to skarn deposits. Introduction - terminology, classification, and composition of skarn deposits. Economic Geology, Seventy-fifth anniversary volume, 1905-1980 77:317-391.

Höck V (1993) The Habach-Formation and the Zentralgneis - a key in understanding the Palaeozoic evolution of the Tauern Window (Eastern Alps) In: Raumer JF, Neubauer F (eds) The Pre-Mesozoic geology in the Alps. Springer, Berlin, pp 361-374.

Höll R, Eichhorn R (2000) Tungsten mineralization and metamorphic remobilization in the Felbertal scheelite deposit, Central Alps, Austria. Rev Econ Geol 11:233-264.

Kozlik M, Raith JG, Gerdes A (2016) U–Pb, Lu–Hf and trace element characteristics of zircon from the Felbertal scheelite deposit (Austria): New constraints on timing and source of W mineralisation. Chem Geol 421:112-126.

Kwak TAP (1983) The geology and geochemistry of the zoned, Sn-W-F-Be skarns at Mt. Lindsay, Tasmania, Australia. Econ Geol 78:1440-1465.

Meinert LD, Dipple GM, Nicolescu S (2005) World skarn deposits In: Hedenquist JW et. al. (eds) Economic Geology, One Hundreth Anniversary Volume 1905-2005. Society of Economic Geologists, Littleton, CO, pp 299-336.

Mulligan R, Jambor JL (1968) Tin-bearing silicates from skarn in the Cassiar District, northern British Columbia. Can Mineral 9:358-370.

Ordosch A (2017) W-Sn mineralisation in calc-silicate rocks of the Basal Amphibolite unit at Messelingscharte (Felbertauern area, Austria). Master thesis, Montanuniversität Leoben, Leoben, pp 188.

Raith JG (1991) Stratabound tungsten mineralisation in regional metamorphic calc-silicate rocks from the Austroalpine Crystalline Complex, Austria. Miner Deposita 26:72-80.

Raith JG, Schmidt S, Aupers K (2018) Field Trip Pre-EX-5. Tungsten deposit Felbertal, Salzburg, Austria. Berichte Geologische Bundesanstalt Wien 126:7-46.

Ribbe PH (1982) Titanite In: Burns BP (ed) Orthosilicates. Mineralogical Society of America, Reviews in Mineralogy, pp 137-154.

Scribner ED, Groat LA, Cempirek J (2017) Mineralogy of the Ash Mountain Sn-bearing skarn, Tuya Range, northern British Columbia, Canada. Can Mineral 55:333-347

Takenouchi S (1971) Hydrothermal synthesis and consideration of the genesis of malayaite. Miner Deposita 6:335-347.

van Marcke de Lummen G (1986) Tin-bearing epidote from skarn in the Land's End aureole, Cornwall, England. Can Mineral 24:411-415.

Vavra G, Frisch W (1989) Pre-Variscan back-arc and island-arc magmatism in the Tauern Window (Eastern Alps). Tectonophysics 169:271-280.

Skarn mineral paragenesis at Delitzsch tungsten occurrence, Central Germany: proximal and distal mineral zoning

Tim Rödel
Economic Geology and Petrology Research Unit, Martin Luther University Halle-Wittenberg, Germany

Bodo-Carlo Ehling
LAGB Sachsen-Anhalt (Geological Survey of the State of Saxony-Anhalt), Germany

Abstract. Determining the local mineral paragenesis and spatial relations of mineral zones is crucial for understanding the structure of intrusion related skarn systems. In the current study archive material from a 1970's drilling program is being used for extensive relogging and detailed petrography. Three main factors control the mineral zonation of the Delitzsch skarn: I) available host rock element inventory II) fluid permeability and reactivity of the host and III) it's distance to the igneous intrusion. The observed systematic mineral zonation has a skewed character with a lateral and vertical component. Laterally it is following a reactive marble layer dipping west at an angle between 45 to 60°. Vertically it is zoned with respect to the interaction of fluids and different host lithologies (hornfels, marble, intrusive rocks). Five main skarn types can be distinguished based on mineral paragenesis and texture. The skarn is forming zones that are often developed concentrically with respect to the vertical and lateral extension. The skarn types might therefore be used for vectoring mineralized sequences occurring proximal to the contact between intrusive rocks and calcic exoskarns.

1 Overview

Defining large scale mineral zones and structures is crucial for understanding intrusion related skarn systems. Amongst other more advanced methods, mapping and petrography of mineral textures and paragenetic relations are the most basic components in explaining the dynamics leading to the formation of skarns (Einaudi 1981; Fonteilles et al. 1989; Kerrick 1977; Meinert et al. 2005; Newberry 1982). The studied mineral occurrence is located in the state of Saxony, Central Germany, less than 5 km southwest of Delitzsch city The area was subject to more than 70 deep exploration drillings starting in the late 1960s. In 1990 the project was stopped due to political reasons and economic considerations. No modern research of the mineralized contact-metasomatic rock sequences has been published in English language (Schenke 1995). The aim of the current study is therefore a) the establishment of detailed description of mineral zones and further b) defining vectors for genetic implications and mineralization. Today archive material from the drilling program is available in different conditions. Eight drill cores with a total skarn intersection of more than 300 m are subject to detailed macroscopic investigations and over 200 petrographic polished sections from a dozen drill holes have been studied up to date. Emphasis was put on creating east-west profiles although drill density is limited to a maximum of three cores on a section. Careful petrography is supported by SEM-EDX analysis using a JEOL JSM 6300 with Bruker X-Flash 5010 detector (123 eV energy resolution) and automated mineralogy using a Hitachi TM4000 Plus with "Advanced Mineral Identification and Characterization System" (AMICS). ICP-MS geochemical data for related igneous rocks and metasomatic skarns was available from previous work. EPMA studies on relevant zoned minerals like garnet, clinopyroxene and scheelite are planned in the future. A first publication with a detailed petrographic description including direct LA-ICP-MS U-Pb dating of garnet is in preparation.

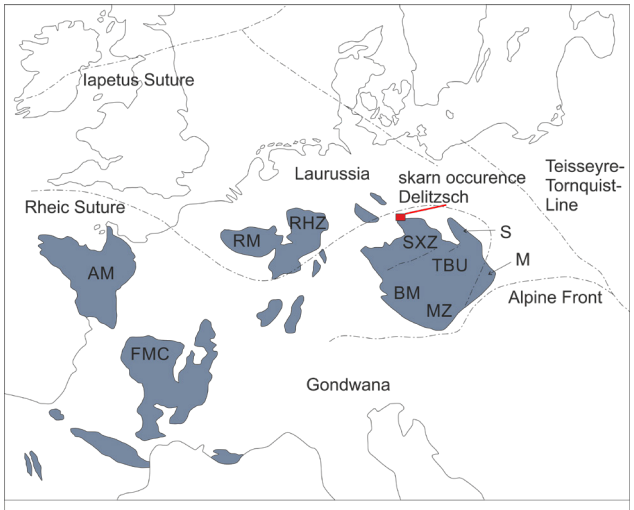

AM Armorican Massif, FMC French Massif C., RM Rhenish Massif, BM Bohemian Massif, RHZ Rheno-Hercynian Zone, SXZ Saxo-Thuringian Zone, TBU Teplá-Barrandian Unit, MZ Moldanubian Zone, S Sudetes, M Moravo-Silesian Zone

Figure 1. Position of the Delitzsch tungsten skarn occurrence in context to the European Variscides (modified from Krüger et al. 2013).

2 Regional geological conditions

The skarn system is positioned at the northernmost margin of the Saxothuringian segment of the central European Variscides in close relationship to the

neighbouring Variscian volcanic arc (Rheic suture) of the Mid-German Crystallin Rise (Fig. 1). A kinked southwest to east trending sedimentary belt (syncline Delitzsch-Torgau-Doberlug) consisting of Cadomian-consolidated Neoproterozoic sediments, Cambrian and Carboniferous sediments were intruded by an igneous intrusion. The area is surficial covered by 100 to 120 m of poorly consolidated Cenozoic glacial and fluvio-glacial sediments. Host rocks of the partly mineralized skarns are alternating carbonatic and pelitic sedimentary sequences of the Lower Cambrian Zwethau-Formation. Intermediate to mafic volcanic and volcano-clastic rocks are interlayered with these sediments. A post-Variscian dated (300-311 Ma) igneous rock suite comprised of diorites, granodiorites and late aplites (Delitzsch pluton) intruded the sedimentary rocks. As a result, the alternating layers of carbonates and pelites of the Zwethau-Formation underwent intense contact metasmorphism. Limestones, dolomitic limestones, pelites and pyroclastics were converted to calcite marbles, dolomite marbles, biotite hornfels and calc-silicate marbles. Infiltration metasomatism appears with the subsequent induction of large volumes of magmatic-hydrothermal fluids into permeable reactive lithologies. Today, the altered sediments with interlayered exoskarns dip westwards in an angle between 60° to 45° roughly parallel to the intrusive contact. As a result, metasomatic skarns occur in a depth between 100 m to 600 m in a roughly 300 m wide zone along a 3 km north-south extension between igneous rocks and contact metamorphosed sediments. The largest continuous metasomatic skarn zones are documented in the investigated southern part of the occurrence. Here, an extensively converted calcite marble sequence with an apparent thickness of 25 to 35 m is developed in-between hornfels. The unit is delimited to the west by compact, impermeable, and less reactive biotite hornfels in the hanging wall and foot wall. To the east the marble unit is completely converted to skarn with discordant intrusion contact in the foot wall accompanied by intense endoskarn formation.

A prognostic ore content of 11 460 MT grading at 0.4 % WO_3 was published by Schenke (1995). The number was later reduced to a third of the original value considering the low drill density and uncertain processability of the ore.

3 Skarn zoning

The observed mineral paragenesis are primarily zoned in dependence to I) available host rock element inventory, II) fluid permeability and reactivity of the host and III) it's distance to the igneous intrusion. Several complex types of mineral zones can be differentiated based on mineral paragenesis and mineral ratios. The term distal and proximal skarn can be used almost synonymous for low and high intensity skarn forming processes.

Due to the inclination of the metasedimentary host, the most distal skarn is found in the west at the highest depth of up to 600 m. To the east, proximal skarn is found directly outcropping beneath Cenozoic cover at around 100 m depth. The intrusive contact might exhibit a steeper dip than the metamorphic layering of the sediments, hereby increasing the distance between skarn and intrusion from 0 m in the east to more than 75 m to the west. The observed mineral zoning of the investigated drill cores appears skewed due to the geological structure and the combination of vertical and lateral zonation. Vertical skarn zoning in a drill hole profile is obviously present due to changes in lithology and the interaction between magmatic hydrothermal fluids and different host rock lithologies during contact metasomatism. Lateral zoning predominantly occurs along the largely metasomatized carbonate sequence with decreasing intensity in distance to the intrusive contact from east to west.

Generally, the skarn is prominently thicker in the proximal zone close to the intrusive contact compared to the distal zone at the marble front. Exoskarn originating from calcic educts is most abundant. Five main types of skarn can be distinguished (a) brown compact fine crystalline garnet-clinopyroxene skarn (or skarnoid) (b) greenish-grey quartz-clinopyroxene-garnet skarn with prominent euhedral crystals floating in quartz matrix (c) medium to coarse crystalline reddish-brown to dark green garnet-skarn with chlorite, calcite and quartz interstitials (d) patchy red-brown to grey albitized garnet-clinopyroxene endoskarn (e) reddish irregular garnet-clinopyroxene exoskarn or skarnoid at the marble front with vesuvianite or prehnite. Locally a more detailed subdivision can be performed. For example, garnet-clinopyroxene skarn (a) might locally have lost most clinopyroxene due to carbonatization forming calcite, actinolite and chlorite. 1.5 m thick granodiorite apophyses intruding the siliceous metasediments can form a dark red garnet skarn which bears little similarity with the corrosive network of endoskarn (d) at the contact between plutonic intrusion and carbonate rich metasediments. Skarn type (a) and (e) were historically called garnetfels (*Granatfels*) due to their compact appearance and fine grained mineral size without clearly visible garnet crystals. *Granatfels* was previously interpreted as reaction skarns forming from localized elemental exchange. Today it can be described as a skarnoid type, forming from slow fluid-rock interaction in less permeable rock sequences.

In the hanging wall and footwall of the metasomatic skarn, bedding parallel clinopyroxene-prehnite-garnet bands are developed in impermeable, compact, and generally non-reactive biotite hornfels. These can be traced up to a distance of at least 150 m away from the skarn. Due to the very localized character of the bands, these are interpreted as metamorphic skarn bands resulting from contact metamorphic triggered diffusion reaction along former fine carbonate layers inside hornfels. They may reach a thickness of 1 m but usually form thin bands of 2 to 8 cm. Rarely, the original carbonate rock is still preserved at the centre of the band whereas a several cm thick, light brown garnet-clinopyroxene skarn is developed in contact to siliceous rock. Hornfels is bleached (loss of biotite) to light grey in contact to high intensity proximal metasomatic skarn.

Bleaching occurs irregularly, cross cutting bedding parallel textures as schlieren or plumes.

Distal skarn is characterized by mineral zones of skarns alternating with pure, well recrystallized calcite marbles or lesser silicate marbles. The contact between skarn and marble is very sharp with a transition zone of not more than 5 cm. Metasomatic calc-silicate zones form several irregular finger shaped apophyses of 20 cm to 2 m reaching into the carbonate wall rocks giving some sections an almost brecciated appearance. The distal skarn (e) is comprised of reddish brown, slightly pinkish calcic garnet with dominant grossular component close to the marble front. Garnet is the main mineral component (more than 70 %) generally forming an anhedral isotropic crystal mass. Euhedral crystal boundaries are sometimes developed close to interstitials. The second most abundant mineral phase is hedenbergitic clinopyroxene which occurs as fine crystal aggregates or single crystals overgrown by grossular. The garnet to pyroxene ration in the distal skarn is around 10:1 to 5:1. Diagnostic for distal skarn at the marble contact is the occurrence of yellowish-brown vesuvianite as subhedral crystals intergrown and sometimes overgrown by garnet. Rarely these minerals occur in some cm distance to the skarn-marble contact in the marble. Particular thin skarn apophyses might contain prehnite or muscovite. Scarce wollastonite with yellowish UV-fluorescence was observed as subhedral lamellar or radiating crystals overgrowing garnet-clinopyroxene skarn at the marble contact. Sulphides rarely occur and are comprised of sphalerite and galena. Skarn sections are more abundant at the hanging wall and footwall boundary, whereas the centre of the altered marble rarely expresses a metasomatic overprint. Close to the hydraulic impermeable hanging wall hornfels, a more continuous, well crystallized andradite dominated skarn (c) with interstitial calcite, chlorite, minor magnetite, and sulphides like pyrite and chalcopyrite forms. Garnet is greenish brown with a yellowish tint and often expresses optical anomal behaviour with oscillatory or sector anisotropy.

Generally, the distal skarn (a or c) is barren of scheelite. Comparably high contents (up to 0.5 % WO_3) were rarely documented in historical reports close to the footwall or hanging wall, sometimes along fractured compact garnet-clinopyroxene skarn (a).

Proximal to the intrusive contact a much thicker skarn sequence with an apparent thickness of up to 60 m is developed. Original carbonate educts were completely converted to a massive skarn succession. The increase in thickness compared to the 25 to 30 m of primary carbonate metasediments could be explained by lithological changes or stacking through faulting. Currently this is supported by little evidence. Texturally it can be explained by the transformation of less reactive hornfels sections to garnet-clinopyroxene skarn (a) in the hanging wall and footwall of the carbonate beds. Whereas the core zone of the profile is dominated by well crystallized, coarse grained garnet skarn (c), zones of euhedral quartz-clinopyroxene-garnet (b) to anhedral garnet-clinopyroxene skarn (a) are enveloping the sequence concentrically. The apparent thickness of skarn (a) is higher in the footwall with zones as large as 20 m to 30 m. Granular garnet skarn replacing the carbonate sequence has an apparent thickness of 30 m. In two drill cores, massive granular garnet skarn (c) is directly outcropping beneath the cenozoic discordance and has a direct intrusive contact, with formation of massive endoskarn (d). As a result, no shell of (a) and (b) type garnet-clinopyroxene skarn is developed.

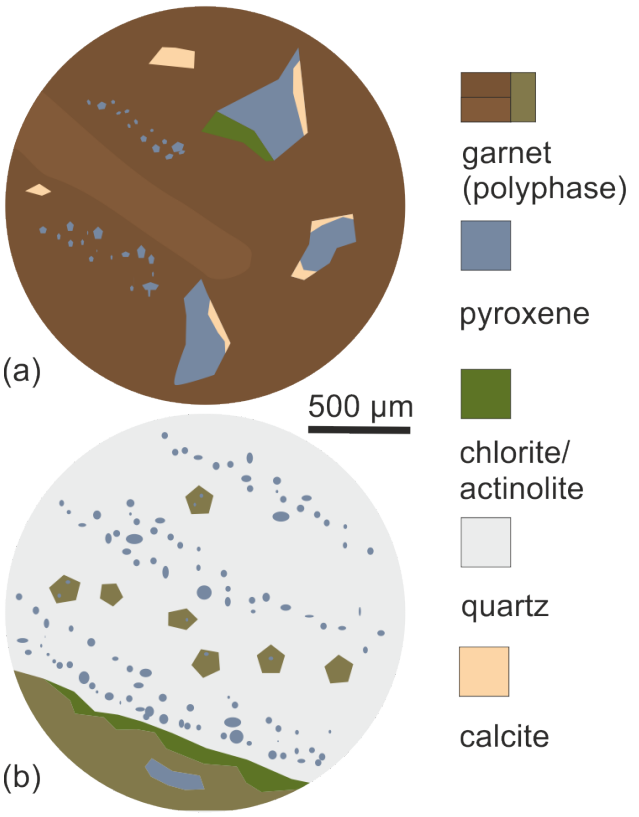

Figure 2. Simplified characteristic rock texture exhibited by garnet-clinopyroxene skarn (a) and quartz-clinopyroxene-garnet skarn (b). Both rock types envelop the granular garnet skarn core zone (c) concentrically.

The outer shell of the proximal skarn consisting of massive compact garnet-clinopyroxene skarn (a) has a brown to reddish brown, rarely light or dark brown homogenous colour (Fig. 2). Textures sometimes appear irregular or cloudy, because of cross cutting reddish or bright late garnet plumes or schlieren. Late garnet might also form discrete bands or veins filled with quartz or calcite rimmed by euhedral red garnet crystals. Clinopyroxene occurs on angular interstitials overgrown by garnet. The ratio of garnet to pyroxene is around 10:1 to 20:1. If altered to calcite, actinolite, and quartz this ratio increases to 50:1. Other minerals occurring interstitially are calcite, chlorite and minor quartz. In clinopyroxene rich areas titanite occurs dispersed. The outer limit of the (a) garnet-clinopyroxene skarn bordering bleached clinopyroxene hornfels can host epidote, prehnite, albite, siderite as well as more abundant chlorite. In the footwall K-feldspar occurs on bands or veinlets. Garnet shows divers composition along the andradite-grossular series with a ratio of Fe to

Al of roughly 1:1 to 4:1.

Occasionally peculiar greenish-grey, mostly fine or medium grained quartz-clinopyroxene-garnet skarn (b) interlayered with minor garnet-clinopyroxene skarn (a) occurs next to the coarse grained main skarn zone (c). It is composed of massive quartz crystals overgrowing minute euhedral clinopyroxene crystals or aggregates and euhedral garnet. Macroscopically the rock exhibits granular and banded texture. Garnet may form aggregates with interlayered clinopyroxene similar to skarn (a). The ratio of garnet to pyroxene is 1:2 to 10:1 in garnet rich bands. Some intervals have exceptionally high epidote, chlorite or actinolite contents. Actinolite forms from the degradation of clinopyroxene in these specific zones. Garnet has fine inclusions of pyroxene or carbonatized pyroxene and often exhibits slight anomal optical anisotropy in the outer rims.

Typical granular, medium to coarse crystalline garnet skarn (c) is forming the core zone of proximal skarn. Grain sizes are commonly larger in the centre compared to hanging wall and footwall. Colours are generally ranging from light brown to dark brown and green to dark green. The granular texture of the skarn is clearly visible due to zonal structure of individual minerals with light core zones and more intensively coloured rims. Texture of the rocks is often massive and not oriented but rarely appears banded by colour changes of light to dark browns and greens. In rare cases, coarse grained (>2 cm) euhedral dark red and dark green, zoned garnet is floating in a quartz matrix along several 50 cm thick bands in the centre of the skarn zone (c).

The coarse grained garnet skarn (c) has a simple mineralogy compared to the distal skarn at the marble front (e) or the enveloping skarns (a) and (b). Garnet is the main rock forming mineral with 75 to 90 % total volume. The amount of garnet might drop to 60 % in zones with high carbonatization or silicification. The garnet often exhibits a strong sectoral or zonal anisotropy which corresponds well to red-brown to dark green growth zones. Optical anisotropy is more pronounced in the centre of the garnet skarn zone (c) compared to the transition closer to garnet-clinopyroxene skarn (a) and (b). Anisotropy is limited to distinct zones on the outer rim of the minerals. In the hanging wall and footwall, a massive thorough anisotropy occurs throughout whole crystals in the coarse grained core zone of the skarn (c). Andraditic garnet is generally more abundant than the grossular-rich variety although a complex compositional oscillatory growth zoning occurs in most crystals. There are drill intervals of red brown or greenish brown massive garnet skarn (c) which do not express any type of optical anisotropy.

Specular hematite is dispersed throughout the skarn (c), forming small radial fillings of interstitials. Chlorite is occurring as dark irregular tattered fillings or patches. It may form intergrowth with massive calcite and quartz interstitials. Sulphides are mainly present as interstitial fillings of chalcopyrite and pyrite. Bi-sulfosalts were observed regularly intergrown with sulphides and hematite.

In contact between calcic exoskarns (c) and the granodioritic intrusive rocks a zone of irregular patchy to amoeboid dark red to grey endoskarn (d) is developed. Close to the contact, intense redbrown Fe-dominant andradite is the main rock forming mineral alongside Fe-rich clinopyroxene, fine grained muscovite, illite, prehnite and fine scapolithe (with yellow luminescence) resulting from the degradation of K-feldspar and albite. Garnet to clinopyroxene ratio is 30:1 to 80:1 closest to the contact and between 7:2 to 5:3 2 m in the footwall. Chlorite occurs regularly whereas epidote is dispersed along K-feldspar-albite-calcite veinlets cross cutting the rock texture.

The only identified W-mineral is the Ca-tungstate scheelite. It is readily identified in the drill core by bright blue fluorescence. Greenish fluorescence is often observed due to a substantial powellite component. The mineralization is disseminated along calcite, chlorite, and quartz interstitials in the transition between the core zone (c) and the garnet-clinopyroxene skarn (a). Subhedral to anhedral crystals and rarely euhedral crystals have been preferably precipitated along bands in fine to medium grained granular garnet skarn zones. WO_3 contents commonly range between 0.2 and 0.6 %. Compact well crystallized quartz-rich garnet skarns rarely host more than 0.1 %WO_3. Scheelite only occurs as minor anhedral inclusions in garnet in coarse crystalline garnet skarn (c) and only accessory in late quartz-calcite veinlets in garnet-clinopyroxene shell (a). In the endoskarn zone (d) scheelite occurs as large fractured amoeboid minerals dispersed along a K-feldspar-albite-calcite vein stockwork.

In the recent study it was demonstrated that the tungsten skarn occurrence Delitzsch in Central Germany displays a systematic complex mineral zonation. Patterns for distal and proximal skarn zones have been established that might be useful for a vectoring purpose. Highest WO_3 grades were observed in the proximal skarn close to the intrusive contact. Vectoring of distal and proximal skarn mineral zones could therefore proof useful in directing future exploration for the strategic metal.

Acknowledgements

The geological survey of the state of Saxony (LfULG) is appreciated for providing sample logistics and Wismut GmbH for allowing the use of historic core log data.

References

Einaudi MT (1981) Skarn deposits. Econ Geo Ann Vol 75:317–391

Fonteilles M, Soler P, Demange M, Derre C, Krier-Schellen AD, Verkaeren J, Guy B, Zahm A (1989) The scheelite skarn deposit of Salau (Ariege, French Pyrenees). Econ Geol 84:1172–1209. doi: 10.2113/gsecongeo.84.5.1172

Kerrick DM (1977) The Genesis of Zoned Skarns in the Sierra Nevada, California. J of Petrol 18:144–181

Meinert LD, Dipple GM, Nicolescu S (2005) World skarn deposits. Econ. Geol. 100:299–336

Newberry RJ (1982) Tungsten-bearing skarns of the Sierra Nevada; I, The Pine Creek Mine, California. Econ Geol 77:823–844. doi: 10.2113/gsecongeo.77.4.823

Schenke G (1995) Über das Wolfram-Molybdän-Erzvorkommen von Delitzsch. Z geol Wiss 23:27–35

District-scale geochemical signatures of calc-silicate skarn minerals from the Pb-Zn (± Ag, Cu) distal skarn deposits in Madan, Bulgaria

Aaron L. Hantsche, Kalin Kouzmanov
University of Geneva; Switzerland

Andrea Dini
Consiglio Nazionale delle Ricerche – Pisa

Rossitsa Vassileva
Geological Institute, Bulgarian Academy of Sciences

Oscar Laurent
ETH Zürich

Abstract. The distal skarn bodies of the Madan ore field provide a unique case study on the chemical evolution of a metasomatic mineralizing system at the regional scale. Despite the lack of a known causative intrusive body, chemical zonation in the skarn bodies suggests more proximal metasomatic replacement and mineralization towards the south. Hosted in marble lenses of the basement rocks, skarn pyroxene crystals show an increase in Fe/Mn ratio by an order of magnitude over a 15km N-S transect. Despite this district-scale trend, pyroxene compositions exhibit a wide range of concentrations at the deposit scale, where the Fe/Mn ratio is controlled by sequential crystallization during skarn formation. These trends correspond with local shifts in grain size and Fe/Mg ratio, and are observed at sample locations across the entire district.

Epidote and other Al-bearing alteration phases, hosted primarily in gneiss, can be sorted into two distinct groups based on major element geochemistry. One phase, Al-rich clinozoisite, maintains the major element chemical signature of the aluminous host rocks, while the second, ferriepidote, forms in veins that cut across the former. Previous work suggests that the secondary epidote may be the coeval metasomatic product of the calc-silicate skarn which formed in the marble, providing additional information for the regional scale chemical patterns.

1 Introduction

The Madan ore field (Fig. 1) in southern Bulgaria is endowed with Pb-Zn (± Ag, Cu) polymetallic deposits expressed as vein, skarn, and carbonate replacement mineralization (Bonev, 1984). The largest of these are hosted by distal pyroxene skarn bodies, the distribution of which is controlled by the intersections between a series of NW trending mineralized faults and marble lenses hosted within the metamorphic basement sequence of the Central Rhodopian dome (Marchev et al., 2005).

In the Madan region, the Central Rhodope Mountains are composed of exposed amphibolite and granulite metamorphic units which were exhumed during post-collisional extension beginning regionally in the Eocene (Bonev et al., 2013). These metamorphic units can be subdivided into: i) an upper unit (Madan), in which marble and amphibolite lenses up to 5-10m thick can be seen as a part of the amphibolite grade metapelite sequence (Bonev, 1984, Burg, 2012), and ii) a lower unit (Arda), higher grade, with relicts of UHP metamorphism, with few or no marble horizons (Marchev et al., 2005). The two tectonic terranes are separated by a low-angle detachment fault, which formed as part of the early extensional regime (Marchev et al., 2005; Burg, 2012, Bonev et al., 2013).

Locally, magmatism associated this extension began with the intrusion of the ~42 Ma Smilian granite (and equivalents to the east), which is interpreted to be displaced by the Central Rhodope detachment (Ovtcharova et al., 2003; Kaiser-Rohrmeier et al., 2004, 2013). Later, rhyolite dikes and ignimbrite deposits were emplaced starting at ~32 Ma and into the Paleogene (Harkovska et al., 1998, Kolkovski et al., 2000; Ovtcharova et al., 2003; Kaiser-Rohrmeier et al., 2004).

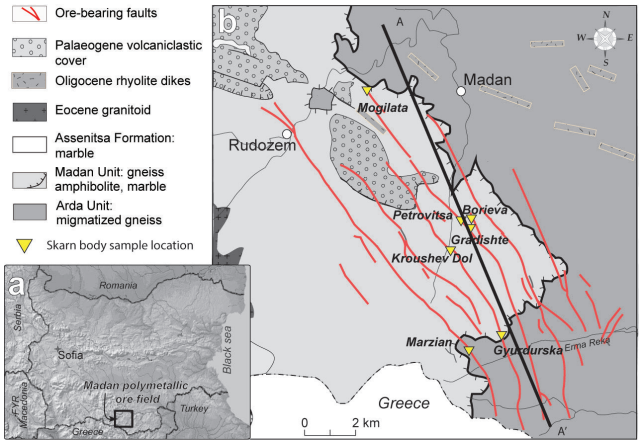

Figure 1. a. Map of Bulgaria. **b.** Simplified geologic map of the Madan ore field (modified from Vassileva et al., 2014)

A rhyolite dike has been used to place an upper age constraint on distal skarn formation based on the cross-cutting relationships with the older dike dated at 31.41 ± 0.39 Ma (U-Pb; zircon; Hantsche et al., 2017). Using late-stage white mica, post-skarn sulfide mineralization in the ore field has a minimum age constraint of 29.95 ± 0.23 Ma (Ar-Ar; sericite; Kaiser-Rohrmeier et al., 2004).

The regional geologic constrains on skarn formation are important to understand the metalogenesis of the district, and the formation of the distal Calc-silicate skarns that host the largest Pb-Zn (± Ag, Cu) ore bodies in the district. The regional geochemical signature of the skarn silicates can help vectoring towards more proximal deposits within the mineralized system.

Skarns

The skarn bodies of the Madan ore field are dominated by Mn-rich clinopyroxene, with garnet skarns observed only as rare occurrences in the southern part of the district (Marzian). The pyroxenes grow as elongate crystals in radial clusters that form dense spheroids with minimal porosity. These skarn bodies are observed in the marble horizons within the Madan tectonic unit, where they are commonly located adjacent to fluid pathways, such as faults, veins, and lithological contacts (Bonev, 1984, Vassileva et al., 2009). Pyroxene skarns extend away from such surfaces into the marble lenses at distances of 10's of meters away from the fluid conduit (Vassileva et al., 2009). More rarely, sub-horizontal and sub-vertical skarn morphologies can be found hosted in marble.

Retrograde alteration of the pyroxene skarn bodies is associated with replacement by amphibole, rhodonite, carbonate, quartz, adularia, and rare garnet. This alteration is often followed by, or is simultaneous with, sulfide precipitation, including sphalerite, galena, pyrite, and chalcopyrite, accompanied by later generations of quartz, calcite, and sericite.

In the aluminous rocks, the skarn-stage alteration is dominated by epidote replacement of the host minerals, but is accompanied by rare garnet occurences. The degree of epidotization corresponds to the distance from the local fluid source (i.e., the vein). Retrograde alteration is present as new epidote crystallization accompanied by sericite and weak sulfide mineralization (sphalerite, galena, pyrite, and chalcopyrite).

2 Methods

We have sampled 7 active and ancient mines (Fig. 1) to observe the district scale variations in major, minor, and trace elements in prograde skarn silicates.

An electron probe microanalyzer (EPMA) at the University of Geneva has been used to determine major element geochemistry. All spot analyses were made at 15kV and 20 nA, with a beam diameter of 1µm. All map analyses were made at 15kV and 100nA, with a 2µm pixel size. Individual pixels from EPMA chemical maps were quantified using XMapTools, calibrated with point analyses within the map area (Lanari et al., 2014; 2018).

Trace element data will be collected using laser ablation inductively coupled mass spectrometry at ETH Zürich using a RESOlution laser ablation system coupled to a ThermoFisher Element XR sector-field mass spectrometer.

3 Results

Results of pyroxene EPMA analyses show chemical distinctions across the longitudinal span of the ore field (~15 km) changing from more Fe-rich compositions in the southern-most mine at Marzian ($Jo_{54}Hd_{35}Di_{11}$), to more Mn-rich compositions in the northernmost deposit at Mogilata ($Jo_{97}Hd_{2}Di_{1}$) (Fig. 2). Grain size variations in the chemistry of pyroxene crystals are also consistent across the district, in which banded pyroxene starts with fine grained (<1cm), Fe-rich crystals with lower Mg/Fe, which grow systematically into larger (up to 5 cm), johannsennitic pyroxene with higher Mg/Fe (Fig. 3).

Epidote geochemistry in samples from the Petrovitsa deposit show two distinct groups, with both an Al-rich and Fe-rich groups. This distinction is associated with epidote derived from host-rock alteration (clinozoisite,) or later vein formation (ferriepidote). Until now, only epidote from the Petrovitsa deposit has been analyzed in this study.

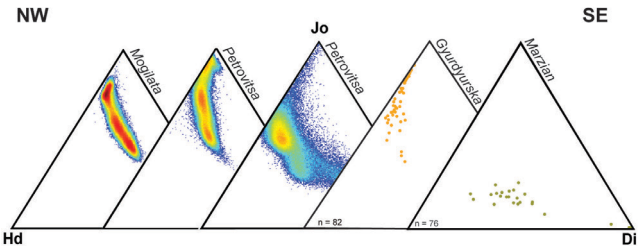

Figure 2. Ternary diagrams of the clinopyroxene solid solution series Johannsenite-Hedenbergite-Diopside. Density plots of pixels from elemental maps generated using XMapTools (Linari et al., 2014; 2018). Gyurdurska (Bovay et al., 2015) and Marzian data from spot analyses.

4 Discussion

Regional patterns of pyroxene compositions indicate the most Fe- and Mg-rich pyroxene compositions from the southern deposits of the Madan ore field (Marzian, Figure 2). However, the variation between johannsennitic (Mn-rich) and hedenbergitic (Fe-rich) pyroxene is not the ideal indicator of proximity to a fluid source, as a wide range of pyroxene compositions exists within individual skarn bodies. The Fe/Mg ratio of the pyroxene crystals may be a more useful tool, as this can be used to differentiate pyroxenes generations in individual deposits (Fig. 3).

"Early" pyroxene crystallizes as fine grain needles with higher concentration of Fe and Mg, but low Fe/Mg ratios. During the crystallization of the pyroxene skarn, larger crystals form radially outward from the early pyroxene (i.e., Marzian), which become higher in Mn

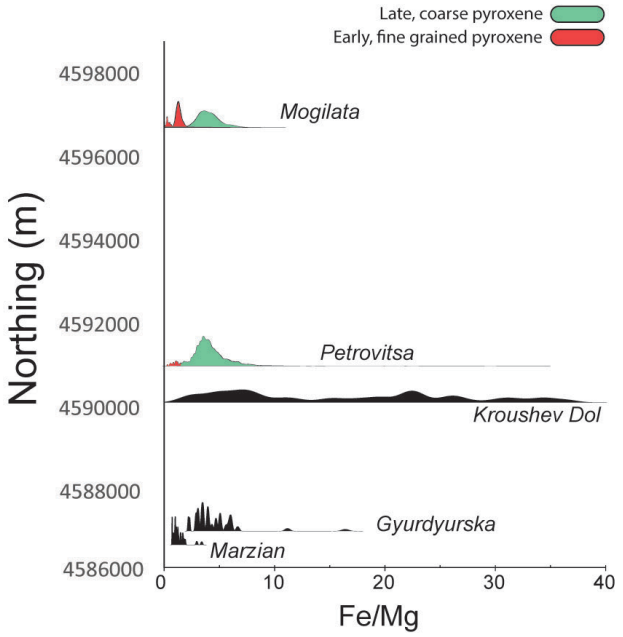

Figure 3. Fe/Mg vs. Northing of pyroxene from 5 deposits. Curves represent probability density functions, where the area under each curve is equal to 1. Unconstrained grain size data presented in black. Kroushev Dol and Gyurdurska data from Bovay et al. (2016).

and are characterized by generally higher Fe/Mg ratios (Fig. 3). The distinct grouping of pyroxene using Fe/Mg ratio provides insight on the chemical banding and compositional variations of pyroxene present at an individual deposit. Bovay et al. (2015) suggested trace element zonation patterns at the local scale that reinforce the observed major element zonation patterns.

Epidote can be grouped into two distinct geochemical clusters (this study; Bovay, 2016). Fe^{3+} - Al^{3+} substitution accounts for this difference, which can be attributed to the host rock in which epidote alteration occurs. Samples from Petrovitsa (altered pegmatite; gneiss) indicate that early, Al-rich clinozoisite, replaces the primary feldspars, versus later epidote, which appears commonly as a vein infill mineral, with a higher Fe/Al ratio. Additionally, previous work on epidote samples from Gyurdyurska which are in equilibrium with prograde or retrograde skarn minerals, have higher Mn concentrations, while retaining the low-Al signature, suggesting potentially syngenetic epidotization of aluminous hosts rocks and Ca-Si skarn formation in carbonate host rocks (Bovay 2016).

5 Early Conclusions and Future Outlook

The district-scale patterns in major element geochemistry of skarn- and skarn-related minerals indicate an increase of Mn and changing Fe/Mg ratios with northward position in the ore field. This helps to quantitatively support work from Vassileva (2004), suggesting more proximal skarn mineralogy and chemistry in the southern extent of the ore field.

Understanding the deposit-scale variations in Fe-Mn-Mg space is critical to decipher the metallogeny of the ore field. Major element geochemical patterns at the outcrop, hand sample, and thin section scales, suggest cyclic skarn growth events in which chemically evolving fluid pulses, along with temperature changes, control concentric chemical banding in skarn silicates.

Similarly, alteration of the host aluminous rocks in the form of epidote presents a promising chemical tracer for processes that may not be recorded by the pyroxene skarns in Madan. The distinction in major element chemistry suggests that the fluids which precipitate the later, Fe-Mn rich epidote, may contain trace element signatures indicative of the fluid source and evolution during transport.

The future aim is to complement the major element geochemistry with trace element compositions (via LA-ICP-MS) from the skarn-related silicates. Local and regional patterns in the silicate chemistry will be linked together to better develop the ore formation model for the Madan ore field. The ultimate goal of this project will be to identify chemical vectors in the skarn minerals to help point towards deeper parts of the mineralized system.

References

Bonev, I. K. (1984) Mechanisms of the hydrothermal ore deposition in the Madan lead-zinc deposits, Central Rhodopes, Bulgaria. IAGOD, pp. 69-73

Bonev, N., Spikings, R., Moritz, R., Marchev, P., Collings, D. (2013). 40Ar/39Ar age constraints on the timing of Tertiary crustal extension and its temporal relation to ore-forming and magmatic processes in the Eastern Rhodope Massif, Bulgaria. *Lithos*, 180:264–278. https://doi.org/10.1016/j.lithos.2013.05.014

Bovay T., Kouzmanov K., Dini A., Wälle M., Vassileva R., Gerdjikov I. (2015) Distal johannsenite-hedenbergite
skarns at Madan, Bulgaria and their link to Pb-Zn mineralization: constraints from trace element analyses in skarn silicates. Swiss Geoscience Meeting-2015, abstract.

Bovay, T. (2016) Distal johannsenite-hedenbergite skarns as an ore-forming environment: Madan, Bulgaria. *MSc. Thesis*, University of Geneva, p.1-138

Burg, J. P. (2012). Rhodope: From Mesozoic convergence to Cenozoic extension. Review of petro-structural data in the geochronological frame. Journal of the Virtual Explorer, 42, 1. https://doi.org/10.3809/jvirtex.2011.00270

Hantsche, A. L., Kouzmanov, K., Dini, A., Vassileva, R., Guillong, M., von Quadt, A. (2017) New U-Pb Age Constraints on Tertiary Magmatism and Pb-Zn Skarn Formation in the Madan district, Central Rhodopes, Bulgaria, Goldschmidt Abstracts, p 1533.

Harkovska, A., Marchev, P., Marchev, Ph., Pecskay, Z. (1998) Paleogene magmatism in the Central Rhodope Area, Bulgaria – A review and new data. *Acta Vulcanologica*, 10:199-216.

Kaiser-Rohrmeier, M., Handler, R., v. Quadt, A., and Heinrich, C.A. (2004) Hydrothermal Pb-Zn ore formation in the Central Rhodopian dome, south Bulgaria: Review and new time constraints from Ar-Ar geochronology. S*chweizerische Mineralogische und Petrographische Mitteilungen* 84:37–58

Kaiser-Rohrmeier M., Von Quadt A., Driesner T., Heinrich C.A., Handler R., Ovtcharova M., Ivanov Z., Petrov P., Sarov S., Peytcheva I. (2013) Post-orogenic extension and hydrothermal ore formation: high-precision geochronology of the central Rhodopian Metamorphic core complex (Bulgaria-Greece). *Economic Geology* 108:691-718

Kolkovski, B., Dobrev, S. (2000) Ore mineralization in the Central Rhodopes. In: Ivanov, Z. (Ed.), Structure, Alpine Evolution and Mineralizations of the Central Rhodope Area (South Bulgaria), ABCD–GEODE 2000 workshop, Borovets. University of Sofia, Bulgaria, pp. 21–42

Lanari, P., Vidal, O., De Andrade, V., Dubacq, B., Lewin, E.,

Grosch, E., Schwartz, S. (2014) XMapTools: a MATLAB©-based program for electron microprobe X-ray image processing and geothermobarometry. Computers and Geosciences. 62:227-240

Lanari, P., Vho, A., Bovay, T., Airaghi, L., Centrella, S., (2018). Quantitative compositional mapping of mineral phases by electron probe micro-analyser. Geological Society of London Special Publication, DOI:10.1144/SP478.4

Marchev, P., Kaiser-Rohrmeier, M., Heinrich, C., Ovtcharova, M., von Quadt, A., & Raicheva, R. (2005). 2: Hydrothermal ore deposits related to post-orogenic extensional magmatism and core complex formation: The Rhodope Massif of Bulgaria and Greece. *Ore Geology Reviews*, *27*:53–89. https://doi.org/10.1016/j.oregeorev.2005.07.027

Ovtcharova, M., von Quadt, A., Frank, M., and Kaiser-Rohrmeier, M. (2003) Triggering of hydrothermal ore mineralization in the Central Rhodopean core complex (Bulgaria)—insight from isotope and geochronological studies on Tertiary magmatism and migmatization, *in* Eliopoulos, D.G., ed*., Mineral exploration and sustainable development*, v. 1: Rotterdam, Millpress: 367–370

Vassileva, R.D. (2004) Compositional variation in the manganoan clinopyroxenes from the Central Rhodopian skarn Pb-Zn deposits, Bulgaria: *Proceedings of the 5th International Symposium on Eastern Mediterranean Geology*, vol III, 1469-1472

Vassileva R.D., Atanassova R., Bonev I.K. (2009) A review of the morphological varieties of the ore bodies in the Madan Pb-Zn deposits, Central Rhodopes, Bulgaria. *Geochemistry, Mineralogy and Petrology* 47:31-49

Vassileva R.D., Atanassova R., Kouzmanov K. (2014) Tennantite-tetrahedrite series from the Madan Pb-Zn deposits, Central Rhodopes, Bulgaria. *Mineralogy and Petrology* 108:515-531

Relative and absolute timing of the KMC Cu-Au skarn deposit in Rogozna Mountains (SW Serbia) using garnets

Irena Peytcheva[1,2], Rafael Burkhardt[1], Albrecht von Quadt[1], Marcel Guillong[1], Dina Klimentyeva[1], Ekaterina Salnikova[3], Maria Stifeeva[3]
[1]Institute of Geochemistry and Petrology, ETH-Zurich, Switzerland
[2]Geological institute, Bulgarian Academy of Sciences, Sofia, Bulgaria
[3]Institute of Precambrian Geology and Geochronology, RAS, St. Petersburg, Russian Federation

Abstract. Grossular-andradites (grandites) of the Karavansalija Mineralized Centre (KMC) in the Rogozna Mountains, SW Serbia, were studied using relative and absolute dating methods. The KMC Cu-Au skarn deposit is a result of multiphase hydrothermal activity caused by discrete magmatic pulses. Shallow magmatic injection of trachyandesites into Cretaceous limestone led to the formation of an extensive prograde exoskarn field followed by retrograde hydrothermal phase that results in a main greenish mass of disseminated "atoll" garnets. Later crowded porphyry stocks and dykes interacted strongly with the skarns reactivating the hydrothermal system. This process led to the formation of endoskarn veins with garnets but also to an enrichment of valuable ore minerals, especially during the retro-grade stage when gold bearing minerals precipitated. All grandites reveal changing chemistry in narrow and/or wide growth zones and variable (<1 to >30 ppm) uranium content. LA-HR-ICP-MS dating yields lower intercept ages of 28.0 ± 1.4 Ma - 26.98 ± 0.75 Ma for the "atoll" garnets and a cross-cutting vein in them and 27.56 ± 0.20 Ma for vein garnets in the crowded porphyry dyke. Consequently, the grandite dating outlines the progress of mineralizing hydrothermal events but is complicated by alteration and overgrowth during the overprinting hydrothermal processes.

1 Introduction

The relative and absolute timing of ore deposits combined with tracing of the dated minerals is crucial for understanding the processes of ore sourcing and deposition and possibly for the general estimation of the economic potential (Rohrlach and Loucks 2005; Chiaradia 2009; Richards 2011; Carrichi et al. 2014; Von Quadt et al. 2018). While the relative timing is based on cross-cutting relationships of rocks, ore veins, and minerals, as well as inclusions in them, absolute dating requires the application of isotopic methods to datable minerals. The Cu-Au porphyry systems are most commonly dated not only because of their economic significance but also due to the possibility to cover the whole range of temperatures during the generation of the deposits (porphyry, skarn and epithermal) from the magmatic to the hydrothermal stages and exhumation (e.g. Chiaradia et al. 2013).

Skarn ore deposits might be part of porphyry systems (Sillitoe 2011) but could also result from a variety of metasomatic processes involving fluids of magmatic, metamorphic, meteoric, and/or marine origin (Meinert et al. 2005). The availability of geochronological data on skarn hydrothermal deposits is rare, due to scarcity of dateable primary skarn minerals. Potential minerals for U-Pb geochronological studies of skarns are the calcium garnets of the andradite-grossular series (grandites). A real revival of the method is connected with the application of the LA-ICP-MS technique (Seman et al. 2017; Wafforn et al. 2018). This is fast and can be applied directly to thin/thick sections or to separated and mounted grains. An important advantage is the possibility to avoid inclusions (if visible), choosing the position of the LA-craters. However, the application of the conventional ID-TIMS U-Pb techniques may provide even more precise age data (Seman et al. 2017; Salnikova et al. 2018) in a case of appropriate grandites.

In present study we are testing the U-Pb garnet dating techniques on the skarns of Karavansalija Mineralized Centre (KMC) in the Rogozna Mountains, SW Serbia (Borojević-Šoštarić et al. 2013 and references therein). Precise CA-ID-TIMS U-Pb zircon dating (Hoerler 2017) revealed 1.7 Ma of magma evolution, skarn formation and about 140 Ka timespan of economic ore mineralization. These results provide a perfect opportunity for comparison with our new geochronological garnet data.

2 Geological setting

The Karavansalija Mineralized Center in the Rogozna Mountains is related to a magmatic suite that is part of the NW-SE oriented Oligo-Miocene Serbo-Macedonian-Magmatic and Metallogenic Belt (SMMMB), which can be traced from Serbia to Macedonia, Bulgaria and Greece (Fig. 1). The belt is represented by Pb–Zn–Ag (± Sb ± Cu ± Au ± W) veined hydrothermal and/or skarn replacement mineralization. A few of the empiric base metal deposits are located within the Rogozna Mts. and in its surrounding areas are the well-known occurrences of Trepca, Crnac, Belo Brdo and Leskova Glava (Borojević Šoštarić et al. 2013; Fig. 1).

Two main magmatic episodes are distinguished in the Cenozoic magmatic complex of Rogozna Mts.: i) an older succession (Ar/Ar ages of about 30 Ma) composed mostly of andesite-dacite ± quartz-latite volcanic rocks, in the eastern part of the complex, and ii) a younger succession (29 to 24 Ma) comprising quartz-latite and related pyroclastics (Borojević-Šoštarić et al. 2013). Borojević-Šoštarić et al. (2012) found numerous

disequilibrium textures, which indicate that the younger rocks formed by crystallization of hybridized magmas. Thus, they concluded a genetic link to the adjacent Pb-Zn-Ag Crnac deposit (~ 5 km north of KMC).

3 Relative timing and the U-Pb CA-ID-TIMS zircon age constraints

The KMC Cu-Au skarn deposit is a result of multiphase hydrothermal activity caused by discrete magmatic pulses. Zircon LA-ICP-MS and ID-TIMS dating together with zircon trace element and Hf isotope measurements suggest that the magmatism started at around 29.3 Ma with andesitic to trachy-andesitic extrusives and shallow intrusive volcanics. Shallow magmatic injection of more evolved trachy-andesites into Cretaceous limestone at ca. 29.0 Ma led to the formation of an extensive prograde exoskarn field. The fluids in excess show 550°C and 55 wt.% NaCl equivalent, indicating a magmatic fluid source. A retrograde hydrothermal phase in the exoskarns led to incomplete reaction of garnet to hydrous phases like chlorite and epidote. After a period of quiescence of about 1.2 Ma, an increased heat and fluid pressure led to the expulsion of fluids from a "crowded" (crystal-rich) porphyritic stock (CP) at ca. 27.76 Ma. They strongly interacted with the skarns establishing/ reactivating the hydrothermal system, which led to the formation of endoskarn veins with garnets but also to an enrichment of valuable ore minerals (arsenic pyrite, chalcopyrite, sphalerite and galena). During the retrograde stage the gold bearing minerals precipitated. Soon after an unmineralized second pulse of porphyry dykes cut the previous "crowded" porphyries and skarns at ca. 27.62 Ma, thus bracketing the maximum timespan of economic ore mineralization to about 140 Ka (Hoerler 2017).

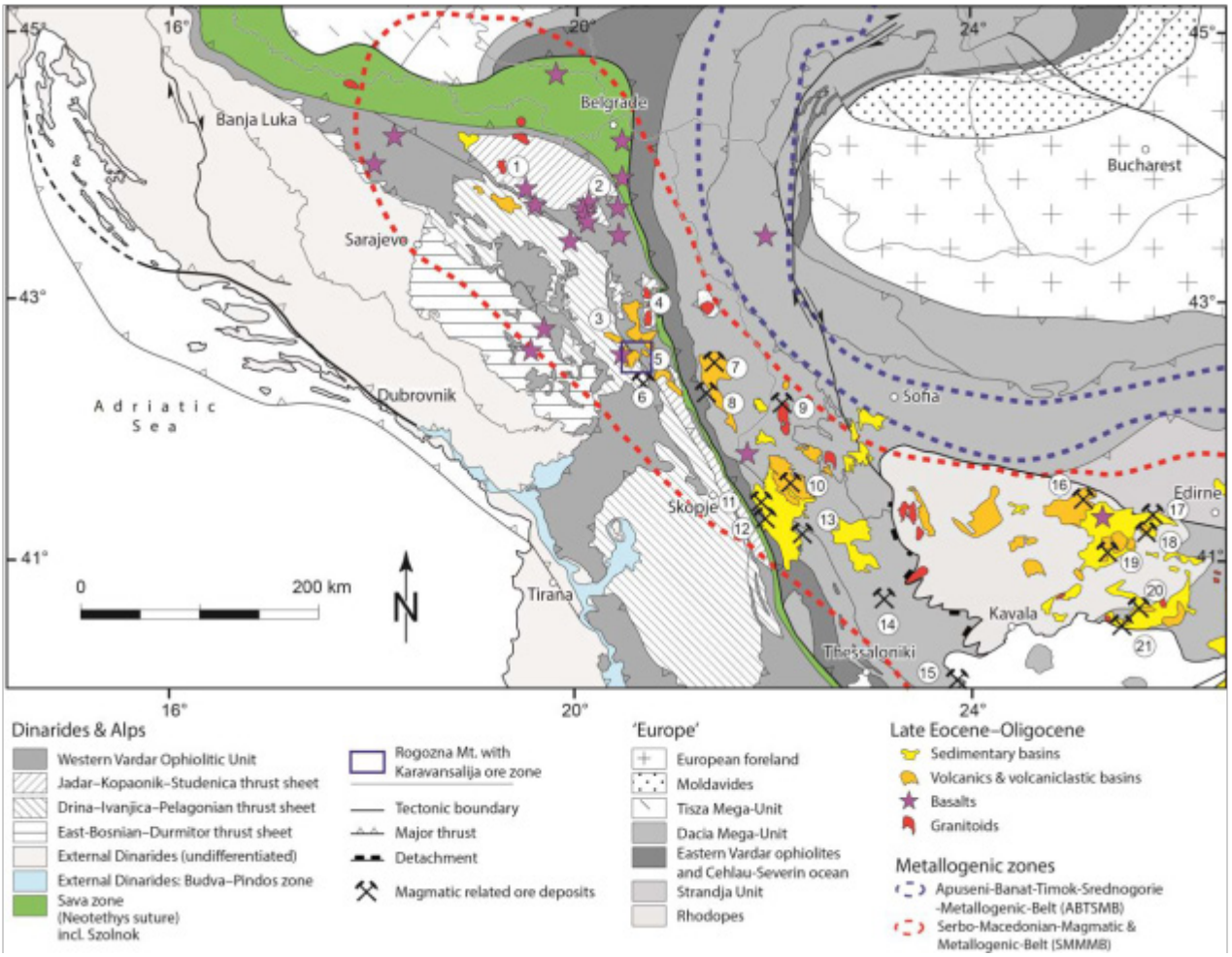

Figure 1. Alpine tectonic units of the Balkan Peninsula (modified after Schefer et al., 2011) with the position of the Oligo-Miocene Serbo-Macedonian-Magmatic and Metallogenic Belt (SMMMB; red dash-line) and the Rogozna Mts. with KMC (purple rectangle). Numbers correspond to important ore deposits of SMMMB: 1 - Veliki Majdan; 2 – Rudnik; 3 – Golija; 4 - Kopaonik & Željin; 5 Karavansalija & Crnac; 6 – Trepca; 7 – Lece; 8 – Kiseljak; 9 – Surdulica; 10 - Kratovo–Zletovo; 11 - Buchim–Damjan–Borov Dol ore district; 12 – Ilovica; 13 – Jekario; 14 – Vathi; 15- Kassandra (Olympias, Mavres Petres, Madem Lakkos, Skouries); 16 – Spahievo; 17 – Lozen; 18 – Madzharovo; 19 - Pcheloyad & Zvezdel; 20 – Sappes; 21 - Perama & Maronia.

4 Garnet sampling

The first group (i) of garnet samples for dating are from the exoskarns related to the early trachyandesitic shallow intrusion. They form a main greenish mass of disseminated “atoll” garnets with chlorite and epidote, which are cross-cut by later Garnet-Quartz-Calcite veins with arsenopyrite. The second group of garnet samples (ii) are from the endoskarn veins in the CP, where they form aggregates and well-shaped muddy orange-greenish crystals.

5 Analytical techniques

EPMA analyses were performed at ETH-Zurich using a JEOL JXA-8200 SuperProbe Electron Probe Microanalyzer. U-Pb isotope and trace element composition of the garnets were defined at ETH Zurich and the Geological Institute of the Bulgarian Academy of Sciences, using a Resonetics Resolution 155 laser ablation system coupled to a ThermoScientific Element HR ICP-MS and UP193FX New Wave LA system and Elan DRCe quadrupole ICP-MS, respectively. Mali (Seaman et al., 2017) and Dashkesan (Stifeeva et al., 2018) garnets were used as primary external standards for dating, and NIST 612 and NIST 610 for trace element analysis. The results were calculated using Iolite combined with VizualAge to obtain ages and ratios corrected for instrumental drift and down-hole fractionation. Iolite or SILLS programs and the SiO_2 content of the garnets (as internal standard or from mineral stoichiometry) are used for calculation of their trace element composition.

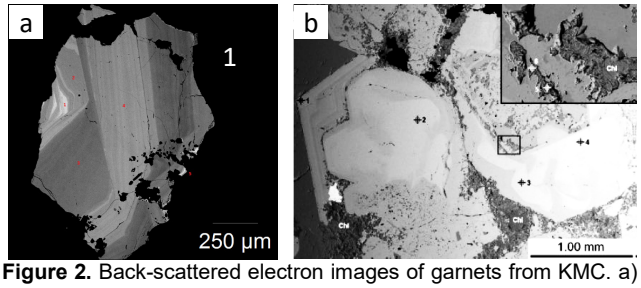

Figure 2. Back-scattered electron images of garnets from KMC. a) type (ii) grossular-andradites; the bright zones correspond to Fe-rich grandites; b) “atoll” grandites type (i) with altered central part, and hydrothermal overgrowths.

6 Results

EPMA analyses of the garnets reveal andradite-grossular ($And_{0.236}Gross_{0.764}$) to end-member andradite composition ($And_{0.998}Gross_{0.002}$) with changing chemistry in narrow and/or wide growth zones (Fig. 2). Typical trace elements are Ti and Mn (0.1-2.6% TiO_2 and 0.1-0.8% MnO). Uranium content is also highly variable (<1 to >30 ppm) with generally higher quantity in grossular-andradites and lower in andradite-grossular and end-member andradite. Chondrite-normalized rare earth (RE) patterns show enrichment in the light to intermediate RE and depletion of the heavy RE (opposite to the patterns of the Fe-series garnets). Other elements in elevated concentrations (compared to C1 chondrite and the trachyandesitic subvolcanics) are Y, W, Nb, P, V, Cr, Ga, Ge, As.

U-Pb garnet age dating with the LA-quadrupole ICP-MS was possible only in the case of U>5-7 ppm and resulted in ages with ≥10% uncertainty. The LA-HR-ICP-MS dating yields lower intercept ages of 28.0 ± 1.4 Ma for the type (i) “atoll” garnets in the exoskarns (Fig. 3), 26.98 ± 0.75 Ma – the vein garnets in the exoskarns, and 27.56 ± 0.20 Ma (Fig. 4) for vein garnets in the crowded porphyry dyke (endoskarns).

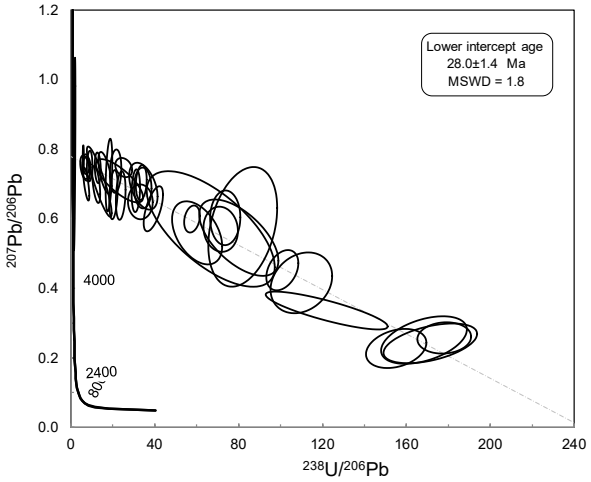

Figure 3. Tera-Wasserburg concordia diagram for exoskarn “atoll” garnets of KMC.

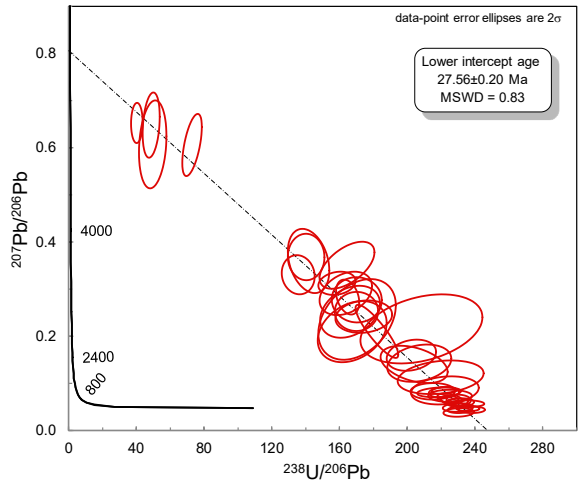

Figure 4. Tera-Wasserburg concordia diagram for type (ii) endoskarn vein garnets of KMC.

ID-TIMS dating of selected grandite grains revealed high common lead contribution and resulted in poorly defined and generally younger ages for all garnet types and samples analyzed.

7 Discussion and conclusions

U-Pb age dating of grossular-andradites of KMC revealed ages that are in agreement with the high precision zircon data. The precision of the garnet LA-

HR-ICP-MS ages (≥1-2% uncertainties) is similar to the one of LA-ICP-MS zircon dating but clearly less precise than the CA-ID-TIMS zircon ages. In the case of KMC absolute timing of the skarn garnets outlines the progress of mineralizing events but is complicated by the hydrothermal alteration, overgrowths and possible Pb-loss during the overprinting process.

As revealed by the relative timing skarification is a multi-stage process. From our garnet U/Pb age it appears that the retrogressive hydrothermal overprint in the exoskarns, formed at 26.98 ± 0.75 Ma, although less precise, is rather contemporary with the progressive and regressive stages of endoskarn than with the main event of skarification in the limestones. We may therefore conclude that the main mineralizing event is related to the crowded porphyry intrusions that postdate the formation of the extensive exoskarns. However, some porphyry dykes cross-cut the mineralized veins and post-date both, the two types of skarns and the Au-Cu-base metal mineralization.

Further potential of skarn garnets in mineral exploration are given through characteristic trace element signatures which is a focus of our ongoing studies.

Acknowledgements

The study is partly supported by ETH-Zurich and projects RFBR-BNSF #18-55-18011 and 02/15, respectively. Special thanks go to the exploration teams of Euromax Services and Eldorado Gold Corporation for the generous access granted to the license area and drill cores and the offered support during the fieldwork.

References

Borojević-Šoštarić S, Cvetković V, Neubauer F, Palinkaš, Bernroider M, Genser J (2012) Oligocene shoshonitic rocks of the Rogozna Mts. (Central Balkan Peninsula): Evidence of petrogenetic links to the formation of Pb-Zn-Ag ore deposits. Lithos 148:176-195.

Borojević-Šoštarić S, Palinkaš L, Neubauer F, Hurai V., Cvetković V, Roller-Lutz Z, Mandić M, Genser J (2013) Silver-base metal epithermal vein and listwanite hosted deposit Crnac, Rogozna Mts., Kosovo, part II: A link between magmatic rocks and epithermal mineralization. Ore Geology Reviews 50:98-117.

Carrichi L, Simpson G, Schaltegger U (2014) Zircons reveal magma fluxes in the Earth's crust. Nature 511:457-461.

Chiaradia M, Schaltegger U, Spikings R, Wotzlaw JF Ovtcharova, M (2013) How Accurately Can We Date the Duration of Magmatic-Hydrothermal Events in Porphyry Systems? Econ Geol 108(4):565–584.

Chiaradia M (2009). Adakite-like magmas from fractional crystallization and melting-assimilation of mafic lower crust (Eocene Macuchi arc, Western Cordillera, Ecuador). Chem Geol 265: 468-487.

Hoerler J (2017) The Karavansalija ore zone at Rogozna Mts. in southwestern Serbia: Magma evolution and time relationship of intrusive events, skarn mineralization and overlying volcanics. MSc Thesis, ETH-Zurich, 77 pp.

Meinert L, Dipple G, Nicolescu S (2005) World skarn deposits. Econ Geol 100th anniversary volume, 299–336.

Richards JP (2011) High Sr/Y arc magmas and porphyry Cu ± Mo ± Au deposits: Just add water. Econ. Geol. 106(7):1075–1081.

Rohrlach BD, Loucks RR (2005) Multi-Million-Year Cyclic Ramp-Up of Volatiles in a Lower Crustal Magma Reservoir Trapped Below the Tampakan Copper-Gold Deposit by Mio-Pliocene Crustal Compression in the Southern Philippines. In: Porter T (ed) Super Porphyry Copper and Gold Deposits: A Global Perspective. Adelaide: PGC Publishing, 270 pp.

Schefer S, Cvetkovic V, Fügernschuh B, Kounov A, Ovtcharova M, Schaltegger U, Schmid S (2011) Cenozoic granitoids in the Dinarides of southern Serbia: age of intrusion, isotope geochemistry, exhumation history and significance for the geodynamic evolution of the Balkan Peninsula. Int J Earth Sci 100:1181–1206.

Seman S, Stockli D, McLean N (2017) U-Pb geochronology of grossular-andradite garnet. Chem Geol 460:106-116.

Sillitoe RH (2010) Porphyry copper systems. Econ Geol 105(1):3-41.

Salnikova EB, Stifeeva M V, Chakhmouradian AR, Glebovitsky V A, Reguir EP (2018) The U–Pb System in Schorlomite from Calcite-Amphobole-Pyroxene Pegmatite of the Afrikanda Complex (Kola Peninsula). Doklady Earth Sciences 478(2):148–151.

Stifeeva M., Salnikova E, Plotkina Y, Peytcheva I, Vassileva R. 2018. Andradite from Dashkesan iron skarn deposit as a potential standard reference material for U-Pb geochronological studies. National Conference with international participation “GEOSCIENCES 2018”, Abstracts, Review of the Bulgarian Geol Soc 79(3):61-62.

Von Quadt A, Large S, Buret Y, Peytcheva I, Heinrich CA (2018) How long does it take to make a giant porphyry copper deposit? Advances in high-precision geochronology and modelling of magmatic-hydrothermal processes. National Conference with international participation “GEOSCIENCES 2018”, Abstracts, Review of the Bulgarian Geol Soc, 79(3):69-70.

Wafforn S, Seman S, Kyle JR, Stockli D, Leys C, Sonbait D, Cloos M (2018) Andradite garnet U-Pb geochronology of the big Gossan Skarn, Ertsberg-Grasberg mining district, Indonesia. Econ Geol 113(3):769–778.

Formation of the Xintianling scheelite skarn deposit, Nanling Range, South China: insights from petrology, mineral chemistry and C-H-O-S-Pb isotopes

Rongqing Zhang, Jianjun Lu, Xudong Huang, Qiang Zhang, Xu Zhao, Xiaoyu Li
State Key Laboratory for Mineral Deposits Research, Nanjing University, China

Abstract. The Xintianling scheelite skarn deposit is situated in the southern Hunan province, Nanling Range, South China. It hosts 0.33 Mt tons of WO_3 and is genetically related to a magnetite-series S-type granitic intrusion, which has high magnetite/ilmenite ratios, high magnetic susceptibility and high zircon Ce^{4+}/Ce^{3+} ratios, distinctly different from the ilmenite-series granites associated with quartz-wolframite-vein type deposits in the Nanling Range. This scheelite skarn deposit was formed at ~162 Ma and is characterized by a mineral assemblage of an oxidized skarn system. It can be divided into five stages: grossular + andradite + diopside (stage I), hornblende + actinolite + Fe-rich andradite + magnetite + scheelite (stage II), scheelite-bearing vein (stage III), molybdenite-quartz vein (stage IV), and calcite + pyrite + sphalerite + galena vein (stage V). Stage II is the dominant scheelite mineralization stage. C-H-O-S-Pb isotopes indicate that the ore-forming fluids are mainly magmatic water mixed with lesser meteoric water and the ore-forming materials are of crustal in origin and derived by mixing of magmatic and sedimentary materials.

1 Introduction

China hosts more than half of the world tungsten resources. The two most important tungsten mineralization belts are Jiangnan Orogeny Belt and Nanling Range, where lots of large tungsten deposits are developed such as Zhuxi (scheelite skarn), Dahutang (veinlet-disseminated scheelite), Shizhuyuan (scheelite skarn and greisen), Piaotang (quartz-wolframite vein), Xintianling (scheelite skarn), Yaogangxian (scheelite skarn and quartz-wolframite vein) and etc.

The Xintianling scheelite skarn deposit is situated in the southern Hunan Province, central part of the Nanling Range, South China. This deposit was discovered in 1957 and detailed prospecting was finished in 1981. It contains 80.9 Mt ore at 0.36% WO_3, 21.8 Mt at 0.022% Mo and 9.5 Mt at 0.033% Bi. Few studies have been conducted to investigate the genesis of the Xintianling deposit (Bi et al. 1998; Cai et al. 2008; Yin and Wang 1994). The petrogenesis of the parental granites, the formation and genesis of the scheelite skarn are still unclear.

2 Petrology of the granitic rocks

The scheelite skarn is spatially related to the Xintianling granite intrusion. The granite intrusion is composed of a central facies of medium-grained biotite granite and a marginal facies of fine-grained biotite granite, cut by granite porphyry dykes (Figure 1). The two granite facies have zircon U-Pb ages of 165.0 ± 3.1 Ma and 164.0 ± 0.6 Ma, respectively, while the granite porphyry dykes have a zircon U-Pb age of 147.5 ± 0.5 Ma. The two facies of biotite granites are metaluminous to slightly peraluminous, and of high-K calc-alkaline compositions. They were formed by fractional crystallization of apatite, monazite, K-feldspar and plagioclase from the same magma system. They have consistent initial $^{87}Sr/^{86}Sr$ ratios of 0.7116 to 0.7198, $\varepsilon_{Nd}(t)$ values −7.1 to −9.5 and zircon $\varepsilon_{Hf}(t)$ values of -4.1 to -11.4, indicative of partial melting of the Cathaysian crustal basement (1.6-1.7 Ga). Granite porphyry dykes cut through the biotite granites and the skarn ore bodies, and have affinities to A-type granite. The dykes have similar initial $^{87}Sr/^{86}Sr$ ratios (0.7123 to 0.7153), slightly higher $\varepsilon_{Nd}(t)$ value (-6.2) and slightly younger Nd and Hf isotopic model ages (1.45 Ga and 1.53 Ga, respectively), suggesting generation by partial melting of Mesoproterozoic metamorphic basement in the lower crust, similar to the earlier granites, but probably involving injection of some mafic mantle-derived magma.

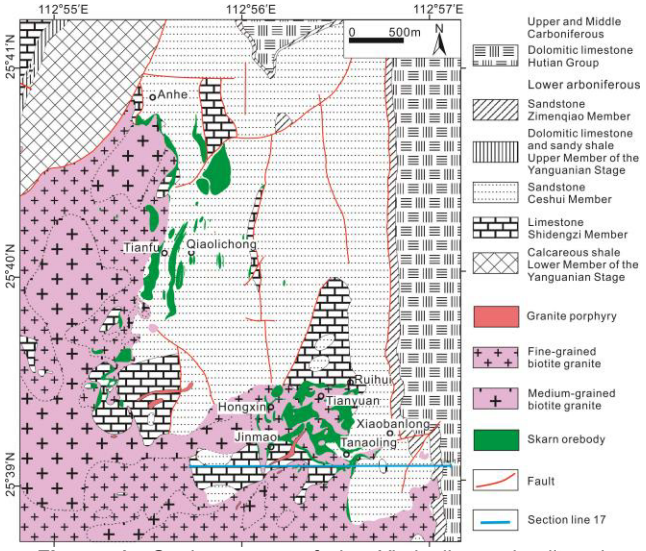

Figure 1. Geology map of the Xintianling scheelite skarn deposit, Nanling Range, South China

The Xintianling biotite granites have an assemblage of magnetite + allanite + titanite, and high magnetite/ilmenite ratio (>4:1), high magnetic susceptibility with an average value of 827×10^{-6} emu/g

and Ce^{4+}/Ce^{3+} ratios in zircon (Figure 2). These features indicate a high oxidation state of the Xintianling granites (magnetite-series), which distinctly differs from most W-bearing granites associated with quartz-woframite vein type deposits in the Nanling Range which are of ilmenite-series affinity. The oxidized nature of the Xintianling biotite granites also implies the absence of mineralization potential of tin.

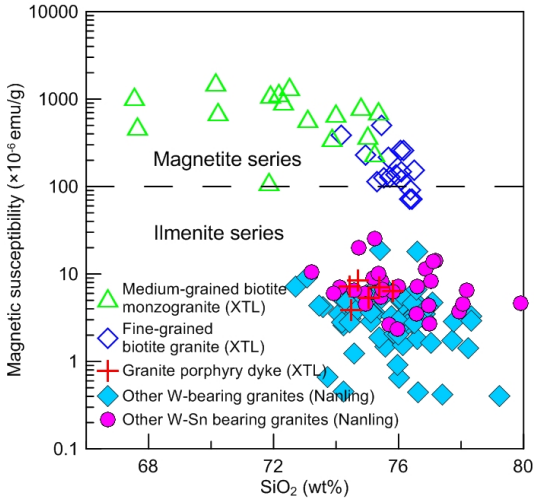

Figure 2. Magnetic susceptibility of the granitic rocks in the Xintianling scheelite skarn deposit and other tungsten deposits in the Nanling Range, South China

3 Mineral chemistry of the scheelite skarn

The orebodies commonly occur in the contact zone between the granite stock and the limestone of the Shidengzi Formation (Yin and Wang 1994). The Xintianling deposit consists of approximately 80 skarn orebodies. Among them, 23 endoskarn, 25 proximal skarn and 32 distal skarn orebodies occur in the granite, at the contact zone and in the limestone, respectively. Endoskarn and proximal skarn are the predominant scheelite ore types, with stratoid, lens- and vein-like shapes. The orebodies are 100~1600 m in length and 1~67 m in thickness, striking nearly north-south and dipping to west at variable angles of 10~80°. Skarn minerals consists of andradite, grossular, diopside, wollastonite, vesuvianite, actinolite, hornblende, epidote, titanite, orthoclase, oligoclase, fluorite, muscovite, and chlorite. The main ore minerals are scheelite and molybdenite, with small amounts of bismuthinite, pyrite, galena, marmatite, azurite, pyrrhotite and limonite. Re-Os dating on molybdenites from skarn and quartz vein yielded an isochron age of 161.8 ± 2.2 Ma. This age is consistent with the zircon U-Pb ages of the host biotite granites within analytical uncertainties, indicating the direct genetic relationship between granitic magmatism and hydrothermal scheelite mineralization.

Several distinct stages of skarnization and mineralization are inferred from paragenetic relationships based on observations of field and thin sections. They can be divided into five broad stages in chronological order: grossular + andradite + diopside (stage I), hornblende + actinolite + Fe-rich andradite + magnetite + scheelite (stage II), scheelite-bearing vein (stage III), molybdenite-quartz vein (stage IV), and calcite + pyrite + sphalerite + galena vein stage (stage V). Scheelite mineralization occurred dominantly as disseminated in stage II and less in veins of stage III. Disseminated scheelite is closely associated with a hornblende + actinolite + magnetite assemblage. In terms of mineral assemblage, three kinds of scheelite-bearing veins can be identified: quartz + scheelite, epidote + fluorite + sphalerite + scheelite and tourmaline + chlorite + scheelite veins.

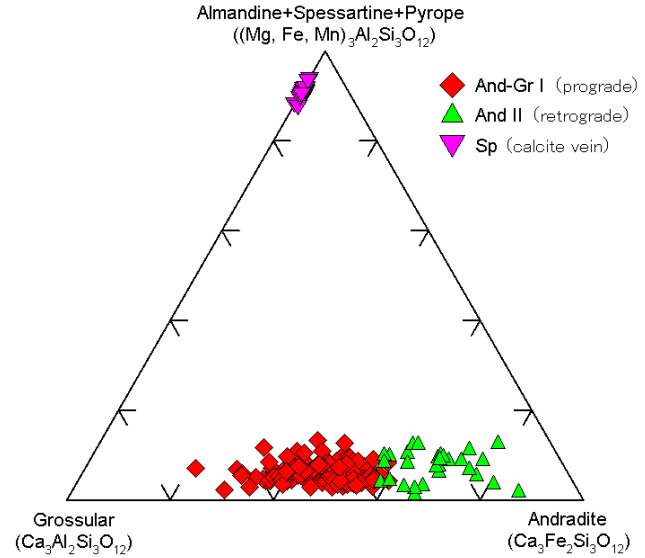

Figure 3. Chemical compositions of garnet from the Xintianling scheelite skarn deposit, Nanling Range, South China

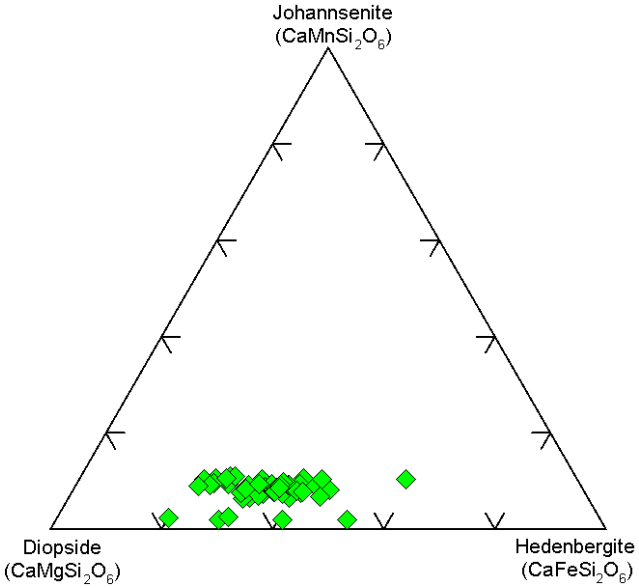

Figure 4. Chemical compositions of pyroxene from the Xintianling scheelite skarn deposit, Nanling Range, South China

Mineral assemblages in stage I indicate oxidized skarn. From stage I to stage II, compositions of garnet change from $And_{31-60}Gr_{38-63}Sp_{3-10}$ (And I) to $And_{58-81}Gr_{10-37}Sp_{1-10}$ (And II) (Figure 3), indicating an increasing trend of Fe-end member and oxygen fugacity. After

replacement by hornblende and actinolite, And II was usually formed around And I. The occurrence of late stage molybdenite mineralization (stage IV) and a calcite + pyrite + sphalerite + galena assemblage (stage V) suggests an oxygen fugacity decrease in post-scheelite mineralization. A small amount of spessartine ($Sp_{72-85}Alm_{6-17}Gr_{7-12}$) associated with sulfides is observed as spessartine-calcite vein in stage I, corroborating further low oxygen fugacity in the late stage. The formation of spessartine is possibly related to the involvement of Mn from the wall rocks. The characteristics of garnet compositions and mineral assemblages in the different stages indicate that scheelite mineralization developed under high oxygen fugacity condition. The compositions of pyroxene are $Di_{46-69}Hd_{20-52}Jo_{2-11}$ (Figure 4). Hornblende and actinolite exhibit narrow Fe-rich and F-poor actinolite rims. Chlorite formed by replacing hornblende and actinolite is dominantly brunsvigite with $Fe^{2+}/(Fe^{2+}+Mg+Mn)$ ratios of 0.26 to 0.4, whereas chlorite in the late stage scheelite veins is mostly ripidolite with $Fe^{2+}/(Fe^{2+}+Mg+Mn)$ ratios ranging from 0.65 to 0.8. Tourmaline is mainly feruvite surrounded by a narrow rim of uvite.

The skarn minerals in the different stages contain extremely low W and no Sn. Mo content in scheelite is less than 0.3 wt% and lower than those in oxidized scheelite skarn of other mines. Scheelite has higher Ce contents (1~2 wt%). Re contents of molybdenite range from 44 ppm to 110 ppm and are higher than those in molybdenite of other scheelite skarn and wolframite-quartz type deposits associated with S-type granite in the Nanling Range, illustrating that Re content in molybdenite is probably influenced by oxygen fugacity of magma.

4 C-H-O-S-Pb isotopes

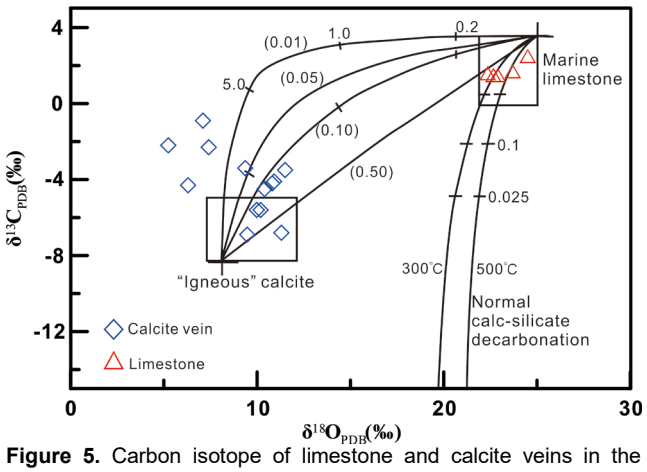

Figure 5. Carbon isotope of limestone and calcite veins in the granite and skarn from the Xintianling scheelite skarn deposit, Nanling Range, South China

The $\delta^{13}C_{PDB}$ and $\delta^{18}O_{SMOW}$ values of limestone are +1.5~+2.5 and +22.4~+24.5, respectively. The $\delta^{13}C_{PDB}$ and $\delta^{18}O_{SMOW}$ of calcite veins in the granite are -5.8~-6.9 and +9.3~+9.5, whereas those of calcite veins in the scheelite skarn are -2.2~-6.8 and +5.2~+11.5. The C-O isotopes of the sedimentary wall rocks and hydrothermal calcite veins indicate that the carbon in skarn was derived by mixing of magmatic carbon and sedimentary carbon (Figure 5).

The $\delta D_{V\text{-}SMOW}$ and $\delta^{18}O_{V\text{-}SMOW}$ values of quartz from the quartz veins in the granite and skarn are -43~-70 and +9.8~+12.3. The calculated $\delta^{18}O_{H2O}$ of fluid inclusions are +2.76~+6.92. As shown in the δD vs. $\delta^{18}O_{H2O}$ diagram (Figure 6), the spots of δD and $\delta^{18}O_{H2O}$ for the quartz fall in or closed to those of the magmatic water, which indicates that the ore-forming fluid was derived by magmatic water mixed with lesser meteoric water.

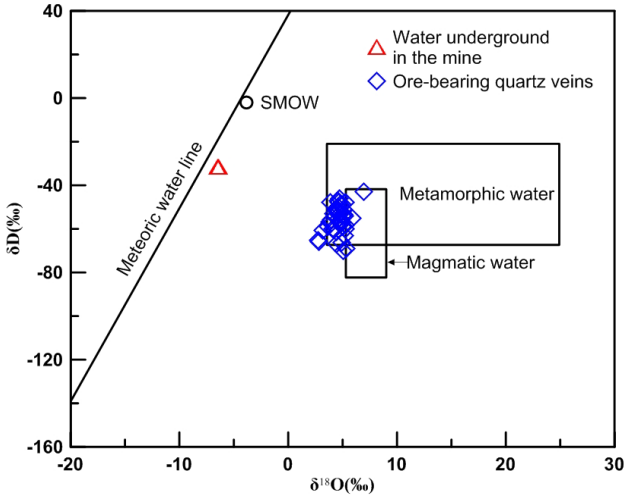

Figure 6. H-O isotopes of quartz from quartz veins in the granite and skarn in the Xintianling scheelite skarn deposit, Nanling Range, South China

The $\delta^{34}S$ values of pyrite and chalcopyrite from the altered granite are -1.5 and +0.7. Disseminated molybdenite in the proximal skarn and molybdenite flakes from the quartz veins have $\delta^{34}S$ values of -1~+1.2. Pyrite and sphalerite from the pyrite-quartz vein and massive pyrite ores in the proximal skarn have $\delta^{34}S$ values of -0.1~+4.6 and +0.32~+3.9, respectively. Pyrite and sphalerite from the massive sulfide ores in the limestone and distal skarn have $\delta^{34}S$ values of +6.3~+8.78 and +7.68~+8.49. The $\delta^{34}S$ values from the distal skarn are +6.1 and +9.04. Sulfur isotopes of sulfides from the Xintianling deposit have two clusters with peaks around 0 and +7 (Figure 7), which indicate the sulfur in the proximal skarn was mainly from the granitic magma and the input of sulfur from the sedimentary wall rocks in the formation of the distal skarn and massive ore in the limestone.

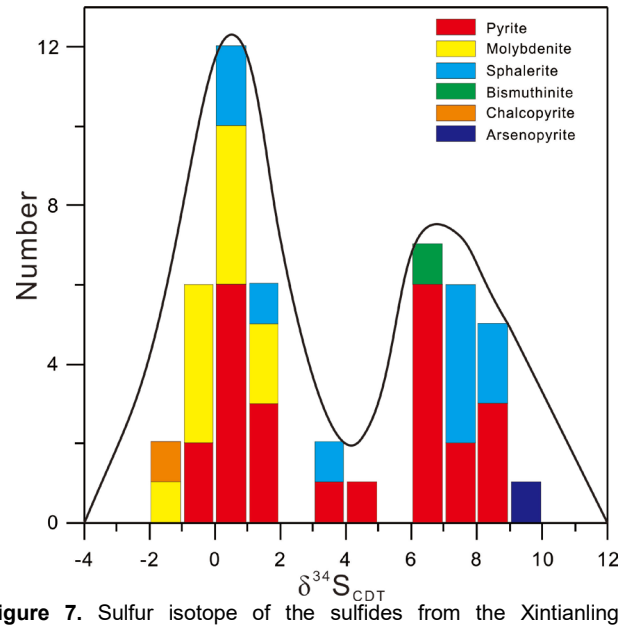

Figure 7. Sulfur isotope of the sulfides from the Xintianling scheelite skarn deposit, Nanling Range, South China

The $^{206}Pb/^{204}Pb$, $^{207}Pb/^{204}Pb$ and $^{208}Pb/^{204}Pb$ ratios of the biotite granites are 18.808~19.377, 15.691~15.758 and 38.922~40.358, whereas the corresponding ratios of granite porphyry dykes are 18.745~19.445, 15.705~15.769 and 39.212~39.839. The $^{206}Pb/^{204}Pb$, $^{207}Pb/^{204}Pb$ and $^{208}Pb/^{204}Pb$ ratios of the sulfides are 18.455~19.595, 15.667~15.828 and 38.748~39.266, whereas those of limestones are 19.330~20.993, 15.689~15.792 and 38.853~38.909. Pb isotopes of all the measured samples fall closed to the evolution line of upper crust, which indicate that the ore-forming materials are of crustal in origin.

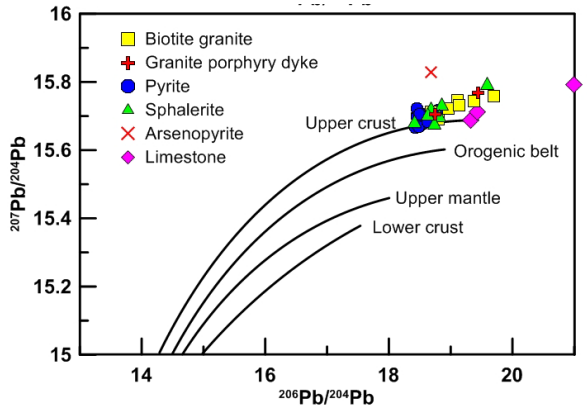

Figure 8. Lead isotope of granites, sulfides and limestone from the Xintianling scheelite skarn deposit, Nanling Range, South China

5 Conclusions

Biotite granites related to the scheelite skarn mineralization in the Xintianling deposit, Nanling Range, South China are oxidized S-type. They have high magnetite/ilmenite ratios, high magnetic susceptibility and high zircon Ce^{4+}/Ce^{3+} ratios.

The formation process of the skarn system can be divided into five stages: grossular + andradite + diopside (stage I), hornblende + actinolite + Fe-rich andradite + magnetite + scheelite (stage II), scheelite-bearing vein (stage III), molybdenite-quartz vein (stage IV), and calcite + pyrite + sphalerite + galena vein (stage V). Scheelite mineralization mainly developed in stage II and was formed at ~162 Ma and

C-H-O-S-Pb isotopes indicate that the ore-forming fluids are mainly magmatic water mixed with lesser meteoric water and the ore-forming material are of crustal in origin and derived by mixing of magmatic and sedimentary materials

Acknowledgements

This study was financially supported by the National Natural Science Foundation of China (41773036, 41830428, 41702092).

References

Bi CS, Wu JS, Wang MY (1988) Stable isotope geology of Xintianling scheelite deposit. Mineral Deposits 7:39-48 (in Chinese with English abstract)

Cai MH, Han FB, He LQ, Liu GQ, Chen KX, Fu JM (2008) He-Ar isotope characteristics and Rb-Sr dating of Xintianling skarn scheelite deposit in Southern Hunan, China. Acta Geol Sin 29:167-173 (in Chinese with English abstract)

Yin SS, Wang CL (1994) Xintianling scheelite deposit in Chenzhou country. Hunan Geol 13:205-211 (in Chinese with English abstract)